CenH3-Independent Kinetochore Assembly in Lepidoptera Requires CCAN, Including CENP-T

Nuria Cortes-Silva, Jonathan Ulmer, Takashi Kiuchi, Emily Hsieh, Gaetan Cornilleau, Ilham Ladid, Florent Dingli, Damarys Loew, Susumu Katsuma, Ines Drinnenberg

CenH3-Independent Kinetochore Assembly in Lepidoptera Requires CCAN, Including CENP-T

Nuria Cortes-Silva, Jonathan Ulmer, Takashi Kiuchi, Emily Hsieh, Gaetan Cornilleau, Ilham Ladid, Florent Dingli, Damarys Loew, Susumu Katsuma, Ines Drinnenberg

Article

Current Biology

CenH3-Independent Kinetochore Assembly in Lepidoptera Requires CCAN, Including CENP-T

Highlights

- Lepidopteran kinetochores lack CenH3 but contain CCAN homologs essential for mitosis
- CENP-I depletion impairs Mis12 and Ndc80 complex recruitment
- CENP-T is sufficient to recruit the Ndc80 and Mis12 complexes
- CENP-T and other CCANs are present in independently derived CenH3-deficient insects

Authors

Nuria Cortes-Silva, Jonathan Ulmer, Takashi Kiuchi, ..., Damarys Loew, Susumu Katsuma, Ines A. Drinnenberg

Correspondence

ines.drinnenberg@curie.fr

In Brief

The lepidopteran kinetochore lacks homologs of CenH3 and CENP-C. Cortes-Silva et al. describe that CENP-T, a newly identified kinetochore protein, and other CCAN homologs are essential for mitotic progression and kinetochore assembly and are conserved in independently derived CenH3-deficient insects.

Cortes-Silva et al., 2020, Current Biology 30, 1–12
February 24, 2020
https://doi.org/10.1016/j.cub.2019.12.014

CellPress

Current Biology
Article

CenH3-Independent Kinetochore Assembly in Lepidoptera Requires CCAN, Including CENP-T

Nuria Cortes-Silva,[1,2] Jonathan Ulmer,[1,2] Takashi Kiuchi,[3] Emily Hsieh,[4,5,6] Gaetan Cornilleau,[1,2] Ilham Ladid,[1,2] Florent Dingli,[7] Damarys Loew,[7] Susumu Katsuma,[3] and Ines A. Drinnenberg[1,2,8,*]
[1]Institut Curie, PSL Research University, CNRS, UMR3664, 75005 Paris, France
[2]Sorbonne Université, Institut Curie, CNRS, UMR3664, 75005 Paris, France
[3]Department of Agricultural and Environmental Biology, Graduate School of Agricultural and Life Sciences, The University of Tokyo, Yayoi 1-1-1, Bunkyo-ku, Tokyo 113-8657,Japan
[4]Molecular and Cellular Biology Graduate Program, University of Washington, Seattle, WA 98195, USA
[5]Division of Human Biology, Fred Hutchinson Cancer Research Center, Seattle, WA 98109, USA
[6]Division of Basic Sciences, Fred Hutchinson Cancer Research Center, Seattle, WA 98109, USA
[7]Laboratoire de Spectrométrie de Masse Protéomique, Institute Curie, PSL Research University, 75005 Paris, France
[8]Lead Contact
*Correspondence: ines.drinnenberg@curie.fr
https://doi.org/10.1016/j.cub.2019.12.014

SUMMARY

Accurate chromosome segregation requires assembly of the multiprotein kinetochore complex at centromeres. In most eukaryotes, kinetochore assembly is primed by the histone H3 variant CenH3 (also called CENP-A), which physically interacts with components of the inner kinetochore constitutive centromere-associated network (CCAN). Unexpectedly, regarding its critical function, previous work identified that select eukaryotic lineages, including several insects, have lost CenH3 while having retained homologs of the CCAN. These findings imply alternative CCAN assembly pathways in these organisms that function in CenH3-independent manners. Here we study the composition and assembly of CenH3-deficient kinetochores of Lepidoptera (butterflies and moths). We show that lepidopteran kinetochores consist of previously identified CCAN homologs as well as additional components, including a divergent CENP-T homolog, that are required for accurate mitotic progression. Our study focuses on CENP-T, which we found to be sufficient to recruit the Mis12 and Ndc80 outer kinetochore complexes. In addition, CRISPR-mediated gene editing in *Bombyx mori* establishes an essential function of CENP-T *in vivo*. Finally, the retention of CENP-T and additional CCAN homologs in other independently derived CenH3-deficient insects indicates a conserved mechanism of kinetochore assembly between these lineages. Our study provides the first functional insights into CCAN-based kinetochore assembly pathways that function independently of CenH3, contributing to the emerging picture of an unexpected plasticity to build a kinetochore.

INTRODUCTION

The centromere is an essential chromosomal region that ensures equal partitioning of chromosomal DNA during cell division [1]. In all eukaryotes, faithful chromosome segregation requires each chromosome to interact accurately with microtubule fibers from the mitotic or meiotic spindle. This interaction is mediated by the kinetochore, a macromolecular protein complex that assembles on centromeric DNA [2]. The centromere-proximal inner kinetochore hosts components of the constitutive centromere-associated network (CCAN), a group of up to 16 different proteins present throughout the cell cycle that create the centromere-kinetochore interface. Upon cell division, the CCAN recruits the centromere-distal outer kinetochore complex, which is composed of the KMN network (Knl1, Mis12, and Ndc80 complex) [3]. This recruitment is enabled by two CCAN subunits, CENP-C and CENP-T, that physically interact with subunits of the Mis12 and Ndc80 complexes [4–11]. The KMN network then mediates the interaction with spindle microtubules to drive chromosome segregation during cell division [12].

Previous work identified the histone H3 variant CenH3 (first identified as CENP-A in mammals [13, 14]) as a core constituent for defining the site of a functional kinetochore in most eukaryotes. This is because CenH3 forms specialized nucleosomes preferentially found at centromeres that are the target sites for kinetochore assembly [15–18]. To do so, CenH3 physically interacts with CCAN components, including CENP-C and CENP-N, connecting the kinetochore to chromatin [19–22]. In addition, attachment of the kinetochore to chromatin can also be facilitated by other CCAN components with DNA-binding activities. In vertebrates and fungi, this includes CENP-C, the direct DNA binding partner of CenH3, and the CENP-T/CENP-W complex, two histone-fold proteins that can form a tetramer with the CENP-S/CENP-X histone-fold dimer [23–25].

Unexpected to its conserved and essential function, CenH3 has been lost in a few select lineages. These include the kinetoplastids [26, 27], which have evolved an entirely different kinetochore complex, and an early-diverging fungus with mosaic centromeres characteristic of both regional and point centromeres [28]. In

addition, our previous studies also revealed the recurrent loss of CenH3 in multiple insect species [29]. Interestingly, these species have also undergone changes in their centromeric architecture in which each lineage independently transitioned from monocentric chromosomes (where microtubules attach to a single chromosomal region) to holocentric chromosomes (where microtubules attach along the entire length of the chromosome). This discovery suggests that these insect species employ an alternative kinetochore assembly mechanism that occurs chromosome-wide in a CenH3-independent manner. Interestingly, despite the loss of CenH3, computational predictions revealed the presence of several CCAN and KMN homologs in holocentric insects [29]. Although those predictions provided some insights into the composition of these CenH3-deficient kinetochores, key aspects of kinetochore function, including how these kinetochores attach to centromeric chromatin and to the outer kinetochore proteins, remained unresolved.

To address these unknowns, we performed proteomics analyses in cell lines from the holocentric Lepidoptera (butterflies and moths). This revealed the presence of several previously unidentified kinetochore components in these insects, including a homolog of CENP-T, a core kinetochore component bridging centromeric DNA to the outer kinetochore in vertebrates and fungi. We show that, in Lepidoptera, CENP-T and other kinetochore components are essential for chromosome segregation and recruitment of the KMN network. Furthermore, we show that homologs of CENP-T are also present in other independently derived CenH3-deficient insects, indicating a conserved mechanism of kinetochore assembly between these CenH3-deficient lineages.

RESULTS

Identification of Kinetochore Components, Including CENP-T, in CenH3-Deficient Lepidoptera

To gain insights into the composition of CenH3-independent kinetochores, we performed immunoprecipitation (IP) experiments of kinetochore components we identified previously in our computational survey [29] (Figure 1A). For this, we established several stable *Spodoptera frugiperda* (Sf9) cell lines expressing 33FLAG-tagged CCAN (CENP-M, CENP-N, and CENP-I) and outer kinetochore (Dsn1 and Nnf1) components to map their protein interaction profiles by mass spectrometry.

Mass spectrometry analyses of the kinetochore immunoprecipitates recovered all of the previously predicted homologs of outer kinetochore and inner kinetochore components, confirming protein complex formation even in organisms that have lost CenH3 (Figure 1B; Figure S1A; Data S1). More importantly, our IPs also revealed several additional components, some of which harbor remote homology to other known kinetochore components (Figure 1B). Among those, we identified a CENP-K-like protein, experimentally supporting previous homology predictions in *Bombyx mori* [31]. We also identified two components (GSSPFG00019785001 and GSSPFG00001205001) with remote similarities to the coiled-coil and RWD (RING finger-containing proteins, WD-repeat-containing proteins, and yeast DEAD [DEXD]-like helicases) domains of the budding yeast CENP-O and CENP-P proteins, respectively. Furthermore, we identified the homolog of the a subunit of the ATP synthase (bellwether, GSSPFG00010096001), found previously to localize to kinetochores during *Drosophila melanogaster* male meiosis [32], indicating that this function might be extended to lepidopteran mitosis.

Both inner and outer kinetochore immunoprecipitates also revealed the presence of a 191.2-kDa protein in *S. frugiperda* (GSSPFG00025035001), with KWMTBOMO06797 being the *B. mori* homolog (Figure 1B). Iterative hidden Markov model (HMM) profile searches within annotated proteomes first revealed homologs in several other insect orders and then known vertebrate CENP-T homologs as best hits (Figure S2A). Similarly, HMM profile searches within known protein structures identified the known *Gallus gallus* CENP-T as the best hit (Figure S2B). The alignment between the lepidopteran and vertebrate CENP-T proteins was restricted to their C-terminal parts that include the histone fold domain (HFD). Importantly, the alignment extended to the known 2-helix CENP-T extension shown to interact with the CENP-H/I/K complex in yeast [33], with several conserved amino acids being identical, supporting homology to CENP-T rather than to any other histone fold protein (Figure 1C; Figure S2C). The sequence aligning with the CENP-T extension appears to be even better conserved than the HFD, allowing identification of *G. gallus* CENP-T in reciprocal HMM profile searches (Figure S2B). Furthermore, analyses of the primary amino acid sequence revealed additional similarities between the *G. gallus* CENP-T and the *B. mori* protein, including enrichment of positively charged amino acids at the N terminus and a proline patch N-terminal of the HFD (Figure 1C). Finally, reciprocal IP experiment of the *S. frugiperda* homolog confirmed its interaction with kinetochore components (Figure 1B). Although orthology between the lepidopteran proteins and CENP-T cannot be confirmed (Figure S2D), the common sequence architecture, kinetochore-protein interaction, and role in outer kinetochore recruitment (see below) lead us to refer to this lepidopteran component as CENP-T.

Interestingly, we could not detect a putative homolog of the CENP-T histone fold binding partner CENP-W in any of our IP experiments, including immunoprecipitates of a 33FLAG-tagged C-terminal truncated version of CENP-T that contains the HFD and 2-helix extension (Figure S1B). Our ability to identify all other known kinetochore homologs in our kinetochore IPs supports the idea that the inability to identify a lepidopteran CENP-W homolog is not due to our IP protocol. However, limitations in detecting those potentially small, arginine-rich proteins by mass spectrometry or incomplete annotations cannot be excluded.

Taken together, we identified previously unknown kinetochore components in the CenH3-deficient kinetochore of Lepidoptera. This includes putative homologs of known CCAN components, including CENP-T. These results reinforce and extend our previous computational predictions indicating similar kinetochore components in Lepidoptera as those in vertebrates and fungi, despite the loss of CenH3 in the former. Among those, the identification of CENP-T was of particular interest because of its known function in DNA binding and outer kinetochore recruitment in other organisms.

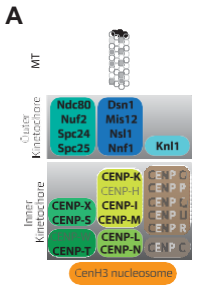

B

				BAIT						
S. frugiperda	*B. mori*	Description	MWG (kDa)	CENP-M	CENP-I	CENP-N	CENP-T	Dsn1	Nnf1	Control
GSSPFG00021458001	LOC101745870	CENP-M	22.0	75 (61.4)	37 (50.3)	1 (8.7)	32 (50.3)	3 (17.3)	12 (27.4)	0
This study	KWMTBOMO02221	CENP-I	76.0	156 (72.9)	110 (55.0)	12 (17.7)	100 (54.9)	26 (29.2)	21 (30.3)	0
This study	KWMTBOMO06206	CENP-N	34.8	67 (72.3)	47 (58.1)	60 (70.0)	38 (44.5)	8 (24.5)	4 (24.5)	3 (24.5)
GSSPFG00023246001	KWMTBOMO11447	CENP-L	34.7	47 (60.0)	39 (48.7)	10 (27.8)	28 (36.1)	5 (19.4)	9 (32.3)	0
This study	KWMTBOMO06797	CENP-T	150.0	137 (40.6)	107 (40.7)	0	127 (40.4)	31(14.7)	18(11.7)	0
GSSPFG00001205001	KWMTBOMO14835	Coil-coiled RWD like protein	51.3	46 (37.6)	28 (25.8)	4 (6.7)	32 (28.8)	6 (6.7)	0	0
GSSPFG00019785001	KWMTBOMO09290	Coil-coiled RWD like protein	43.9	53 (40.1)	49 (30.1)	0	44 (29.3)	2 (6.7)	2 (6.2)	1 (3.8)
GSSPFG00011797001	KWMTBOMO06154	unknown	28.0	33 (64.9)	41 (59.1)	5 (25.3)	33 (53.3)	4 (21.2)	3 (16.2)	0
GSSPFG00006732001	LOC101741561	CENP-K-like	38.3	16 (50.2)	23 (43.4)	1 (6.9)	16 (41.6)	1 (3.5)	3 (10.4)	0
GSSPFG00010096001	KWMTBOMO11351	ATP synthase alpha subunit	59.5	0	20 (29.5)	11 (26.3)	21 (27.9)	9 (23.4)	0	0
GSSPFG00019290001	KWMTBOMO11557	unknown	116.9	22 (21.4)	1 (1.0)	1 (1.8)	0	18 (17.3)	19 (17.4)	0
GSSPFG00032316001	KWMTBOMO08735	Dsn1	20.8	0	0	0	0	17 (37.6)	10 (27.0)	0
GSSPFG00008460001	KWMTBOMO10952	Nnf1	25.6	0	0	0	0	32 (49.5)	21 (44.5)	0
GSSPFG00031222001	KWMTBOMO01237	Mis12	23.1	0	0	0	0	39 (61.8)	21 (52.9)	0
SFRICE018641	KWMTBOMO14775	Nsl1-like	15.5	0	0	0	0	46 (77.8)	22 (62.2)	0
SFRICE020972	KWMTBOMO14865	Spc24	10.9	0	0	0	0	3 (11.4)	1 (5.7)	0
GSSPFG00007708001	KWMTBOMO10335	Spc25	25.2	0	0	0	0	5 (17.5)	6 (33.6)	0
GSSPFG00005966001	KWMTBOMO04152	Ndc80	73.2	0	0	0	0	42 (40.1)	38 (38.1)	0
GSSPFG00010779001	KWMTBOMO07070	Nuf2	40.9	0	0	0	1 (4.5)	11 (38.7)	13 (36.7)	0
GSSPFG00000064001	KWMTBOMO14736	Knl1	186.3	1 (1.0)	0	0	0	108 (38.6)	78 (27.0)	0

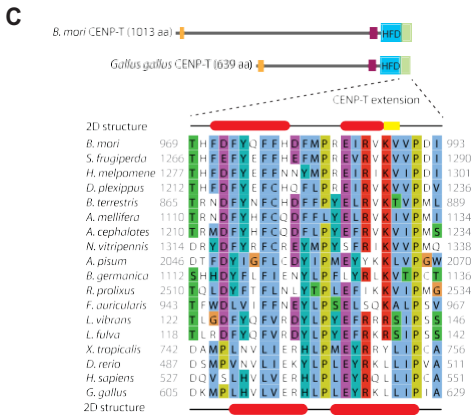

Figure 1. Identification of Kinetochore Components, Including CENP-T, in CenH3-Deficient Lepidoptera

(A) Schematic kinetochore organization in vertebrates and fungi. Boxes indicate subcomplexes within inner and outer kinetochores. Kinetochore components present in Lepidoptera are highlighted in bold ([29], this study). Kinetochore components that cannot be identified or with limited homology are shown in gray.

(B) The table lists the number of peptides and coverages (in parentheses) of known kinetochore homologs or *S. frugiperda* proteins identified by mass spectrometry that were enriched in at least three of the kinetochore IPs over the control. Samples were boiled from the beads, and the analyses were performed on the entire sample. The corresponding homologs in *B. mori* and descriptions based on homology predictions are listed alongside. See also Data S1 and Figure S1.

(C) Top: graphical representation of the *B. mori* CENP-T and *G. gallus* CENP-T sequence features, showing the location of the HFDs (blue box), CENP-T family-specific extension (green box), and arginine-rich (*E* value 4.7 3 10^{-5} and *E* value 6.0 3 10^{-7}, respectively) and proline-rich regions (*E* value 3.7 3 10^{-4} and *E* value 3.4 3 10^{-8}, respectively) (orange and purple boxes, respectively). Bottom: multiple alignment of the C-terminal extension of vertebrate and insect CENP-T proteins. *B. mori* (top) and *G. gallus* (bottom) secondary structure predictions are derived from Jpred4 (a-helical regions are shown in red and b strands in yellow) [30]. Background coloring of the residues is based on the ClustalX coloring scheme. Full-length insect CENP-T sequences and accession numbers, where available, are listed in Table S1. See also Figure S2.

CENP-T and Other Kinetochore Components Are Required for Accurate Mitotic Progression

In other organisms, depletion of kinetochore components results in mitotic defects [34]. Previous studies in *B. mori* have shown that, consistently, depletion of outer kinetochore components also results in mitotic defects and increased numbers of aneuploid cells [35]. We extended this previous study by using RNAi to deplete a broader catalog of kinetochore components. Namely, we depleted several outer kinetochore components of the Mis12 complex (Dsn1, Mis12, and Nsl1) and the Ndc80 complex (Spc24 and Spc25) as well as several inner kinetochore components (CENP-T, CENP-I, CENP-M, and CENP-N). We characterized the resulting mitotic phenotypes by immunofluorescence (IF) at two time points (3 and 5 days). We further validated the efficiency of our kinetochore mRNA depletions by RNA blot analyses (Figure S3A).

RNAi-mediated depletion of all kinetochore proteins tested resulted in an increase in the number of mitotic cells relative to the control (RNAi targeting GFP), indicating that kinetochore-depleted cells are delayed or arrested in mitosis. We observed the strongest increase of mitotic cells upon CENP-T, CENP-I, and outer kinetochore depletion, whereas milder enrichment was seen upon CENP-M and CENP-N depletion (Figure 2B). Interestingly, although still above control levels, the mitotic indices upon CENP-I, Spc24, and Spc25 depletion were strongly decreased at a later time point (Figure S3B), suggesting that, possibly, cells can exit from mitosis and continue progressing through the cell cycle or undergo apoptosis.

In addition to the elevated mitotic indices, depletion of kinetochore components results in various degrees of mitotic defects in these cells (Figures 2C and 2D; Figures S3C–S3F). Here, approximately one-fourth of CENP-T-depleted mitotic cells displayed misaligned monopolar

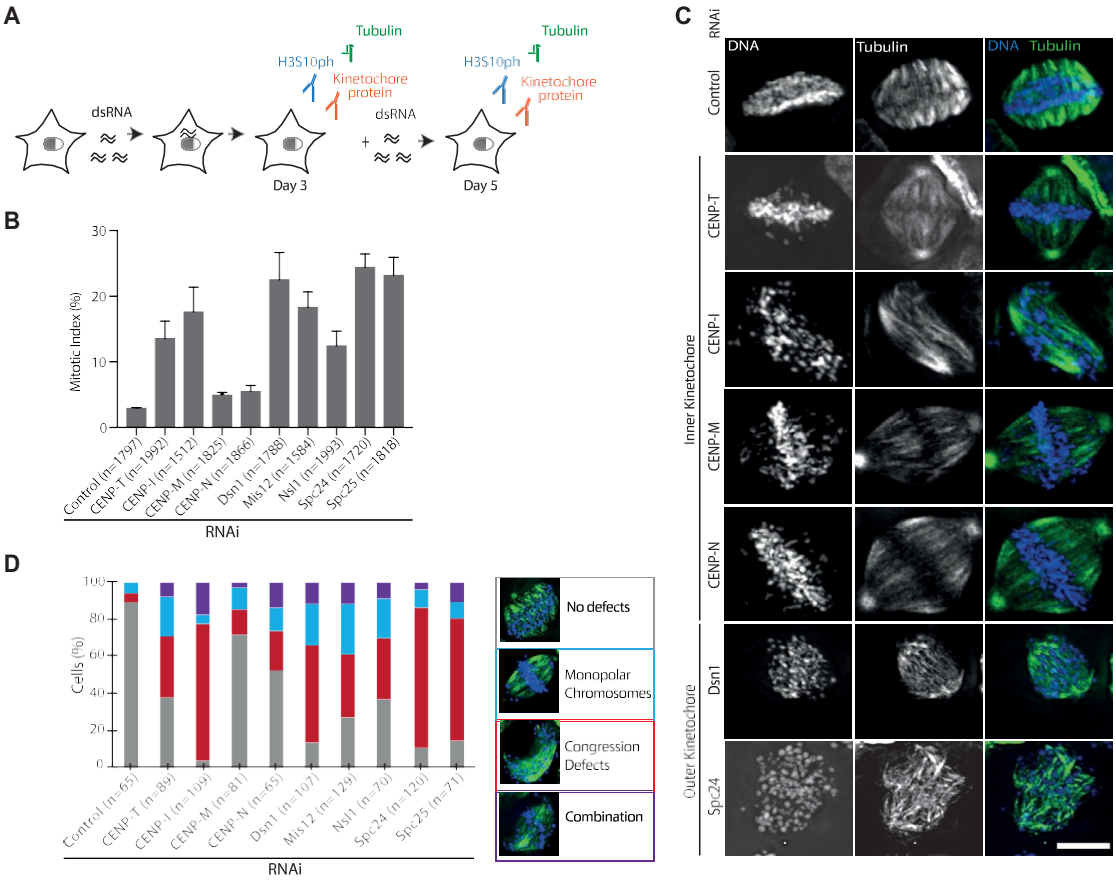

Figure 2. Depletion of Kinetochore Components Affects Mitotic Progression in *B. mori* Cells

(A) Schematic of the RNAi-mediated depletion strategy. BmN4-SID1 [36] cell lines engineered for properties of enhanced uptake of dsRNA were incubated with various dsRNA constructs for targeted depletion of kinetochore transcripts. After 3 and 5 days, cells were analyzed by IF staining against anti-tubulin and anti-phospho histone H3-Ser10 (H3S10ph) in combination with each of our custom-made antibodies against the kinetochore protein of interest. The growth medium was changed on day 3 to add new dsRNA. The efficiency of kinetochore transcript depletion was confirmed by RNA blot analyses (Figure S3A).

(B) Graph showing the percentage of mitotic cells (H3S10ph-positive cells) 3 days after RNAi-mediated depletion of targeted kinetochore components (n = number of cells ± SEM). For results on day 5, see Figure S3B.

(C) Representative images of mitotic cells stained with anti-tubulin (green), used to classify mitotic defects observed 3 days after depletion of select kinetochore components. Scale bar, 10 mm. For results on day 5 and depletion of additional outer kinetochore components, see Figures S3C and S3D. For a zoomed-out version, see Figures S3E and S3F.

(D) Percentages of cells showing no defects (gray), monopolar chromosomes (blue), congression defects (red), and both defects (combination, purple) (n = number of cells analyzed per condition) for different kinetochore depletion experiments.

chromosomes (where one or several chromosomes are not aligned at the metaphase plate and remain at the spindle pole). In addition, 34% of CENP-T-depleted mitotic cells showed complete failure of chromosomes to congress at the metaphase plate (Figures 2C and 2D). This phenotype was even more pronounced upon CENP-I, Spc24, and Spc25 depletion, with the majority of cells (73%, 76%, and 66%, respectively) unable to successfully congress chromosomes (Figures 2C and 2D). In contrast, mitotic defects upon CENP-M and CENP-N depletion (Figures 2C and 2D) were relatively mild but became more pronounced at the later time point (Figures S3D–S3F). These results show that all tested inner and outer kinetochore components are required for high-fidelity chromosome segregation in *B. mori* cells. Additionally, the defects observed upon depletion of the newly identified CENP-T further support its role in chromosome segregation, which we aimed to analyze further.

The CENP-T N- and HFD-Containing C Termini Are Essential for Accurate Mitosis

We next tested whether we could rescue CENP-T knockdown phenotypes by complementation with an RNAi-resistant version of CENP-T. Using double-stranded RNA (dsRNA) targeting the endogenous CENP-T transcript and a FLAG-tagged recoded CENP-T construct unable to be targeted by the dsRNA, we were able to selectively deplete *B. mori* cells of endogenous CENP-T but not FLAG- tagged CENP-T (Figure S4). These experiments were more qualitative than quantitative because of the low transfection efficiency in lepidopteran cells in combination with low

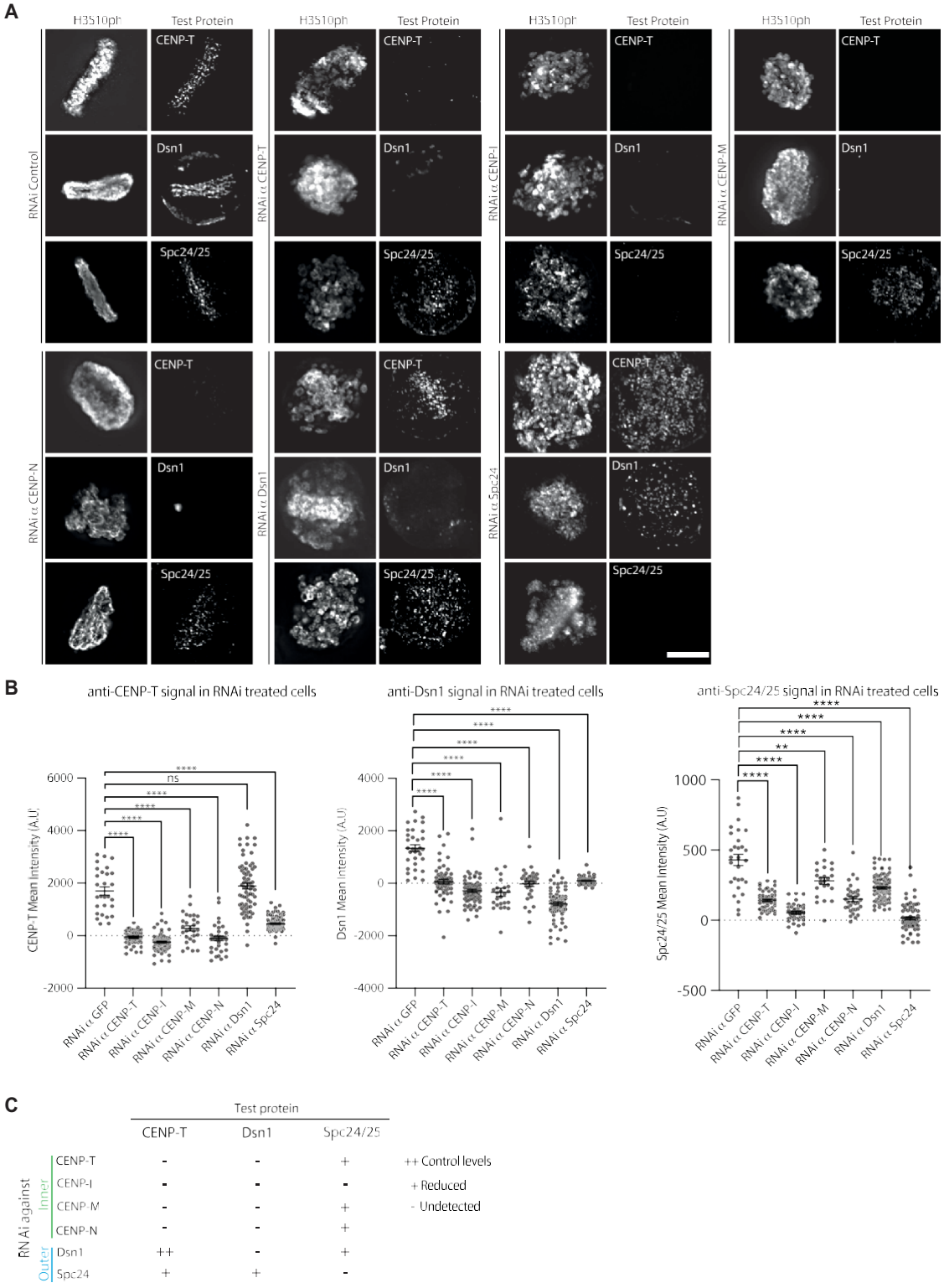

Figure 3. Depletion of CCAN Components Affects CENP-T and Outer Kinetochore Recruitment in *B. mori* Cells

(A) Representative images of mitotic BmN4-SID1 cells, showing the levels of endogenous CENP-T, Dsn1, and Spc24/Spc25 with and without depletion of inner (CENP-T, CENP-I, CENP-M, and CENP-N) and outer (Dsn1 and Spc24) kinetochore components. Scale bar, 10 mm.

(legend continued on next page)

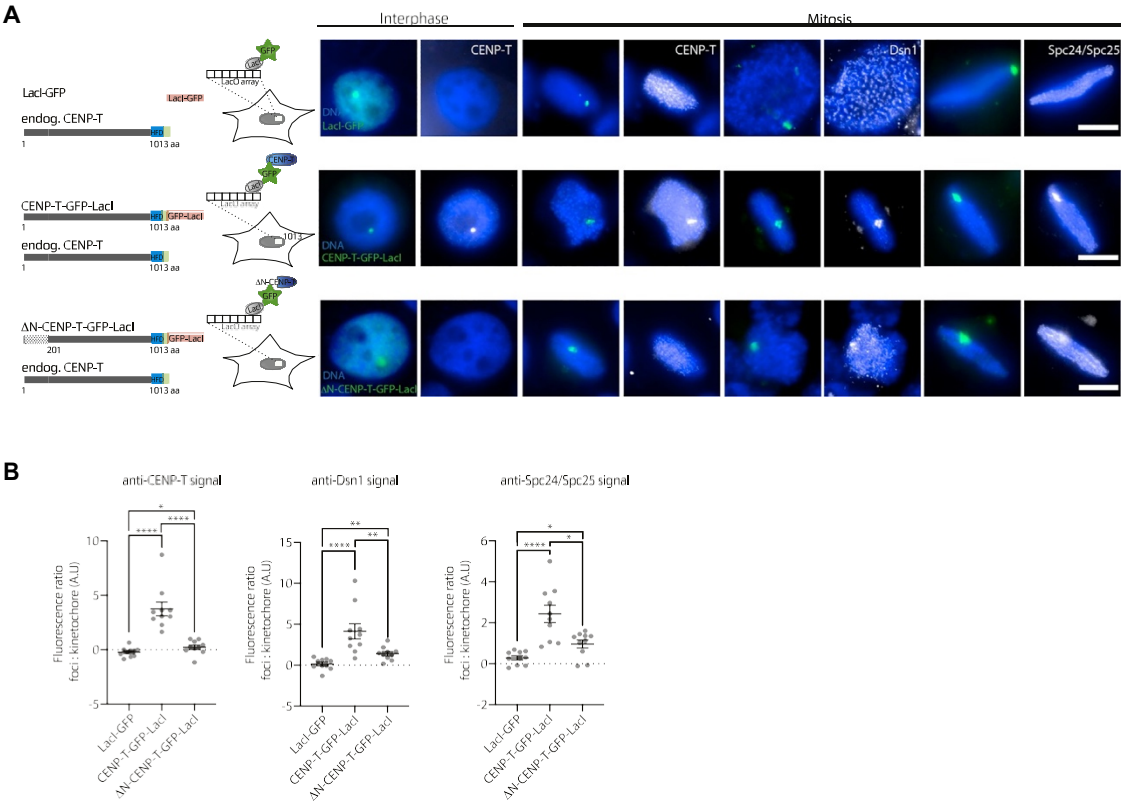

Figure 4. Ectopic CENP-T Is Sufficient to Recruit the Outer Kinetochore in *B. mori* Cells

(A) Representative images showing localization patterns of endogenous CENP-T, Dsn1, and Spc24/Spc25 (gray) in BmN4-LacO cells transiently expressing LacI-GFP (top row), CENP-T-GFP-LacI (center row), and DN-CENP-T-GFP-LacI (bottom row) constructs (green). Scale bars, 10 mm.

(B) Quantifications of mean fluorescence intensity of CENP-T, Dsn1, and Spc24/Spc25 at GFP foci versus CENP-T, Dsn1, and Spc24/Spc25 at endogenous sites (n = 10 cells analyzed). The ratios of mean fluorescence intensities on GFP foci over endogenous loci are shown. Statistical significance was tested using a Mann-Whitney test (****p % 0.0001, **p % 0.01, *p % 0.05).

See also Figure S5.

numbers of mitotic cells that could be analyzed. Still, among the cells that could be analyzed, expressing the full-length RNAi-resistant construct (CENP-Tres-FLAG) rescued the mitotic defects described above (Figure S4). In contrast, cells expressing the wild-type, non-resistant construct (CENP-T-FLAG) displayed mitotic defects, as observed previously (Figure 2). To evaluate whether the N- or HFD-containing C terminus of the CENP-T protein or both are required for its function, we expressed RNAi-resistant FLAG-tagged N- and C-terminally truncated CENP-T constructs (DN-CENP-Tres-FLAG and DC-CENP-Tres-FLAG, respectively). Cells expressing either of the two constructs failed to rescue the observed mitotic defects (Figure S4), leading to the conclusion that the full-length CENP-T protein is necessary for accurate mitosis.

Accurate Localization of CENP-T Is Dependent on Other Inner Kinetochore Components and Is Necessary to Recruit the Mis12 Complex

Next, to evaluate the role of CCAN and outer kinetochore components in kinetochore assembly, we depleted individual kinetochore proteins and stained with custom-made antibodies against the lepidopteran CENP-T, Dsn1 (Mis12 complex), and Spc24/Spc25 (Ndc80 complex). We validated the specificity of the antibodies by mass spectrometry, western blot analyses, and IF upon RNAi-mediated depletion of the respective genes (Figure 3A; Figure S5).

As expected for kinetochore components, we observed the immunosignals of CENP-T, Dsn1, and Spc24/Spc25 co-localizing with mitotic chromosomes (H3S10ph-positive cells) in control BmN4 cells (RNAi targeting GFP) (Figure 3A). We then

(B) Quantification of mean fluorescence intensity for CENP-T, Dsn1, and Spc24/25 signals in the control or upon kinetochore depletion. Statistical significance was tested using a Mann-Whitney test (****p % 0.0001, ***p % 0.001, **p % 0.01, *p % 0.05). For depletion of additional outer kinetochore components, see Figure S6.

(C) Table summarizing the centromeric localization results of endogenous CENP-T, Dsn1, and Spc24/25 upon RNAi depletion. ++ represents control levels, + represents reduced fluorescence levels compared with control levels, and – refers to undetected levels.

See also Figures S4 and S5.

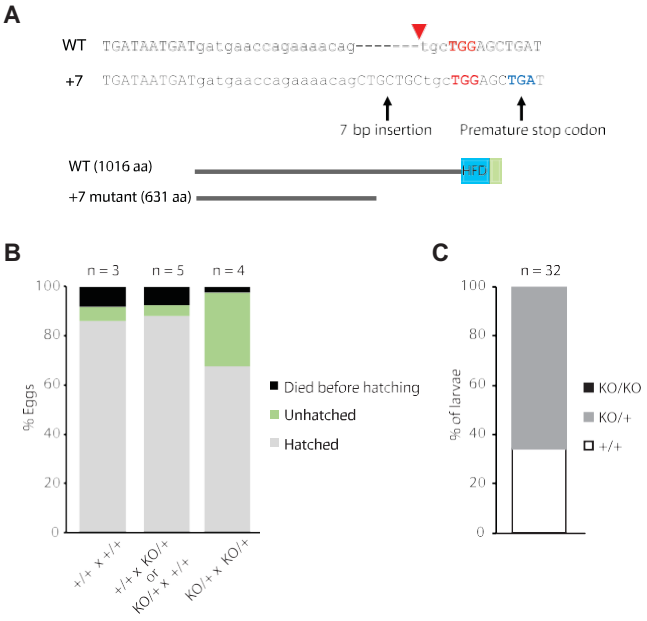

Figure 5. The *B. mori* CENP-T Protein Is Essential *In Vivo*

(A) CRISPR/Cas9-introduced mutation in the Cenp-T coding sequence. Top: alignment between wild-type (WT) and mutant (+7) sequences, showing a 7-bp insertion of the Cenp-T gene. Bottom: schematic of WT and truncated protein products in the CRISPR mutant. The PAM site (red), premature stop codon (blue), and Cas9 cleavage site (red arrow) are indicated.

(B) Hatching rate of the WT and Cenp-T mutant strains. The percentages of hatched (gray), unhatched (green), and eggs that died prior to hatching (black) are indicated for the different crossing patterns between WT (+/+) and heterozygous Cenp-T mutants (+/knockout [KO] or KO/+). The number of independent crosses (n) is shown above. The raw data are shown in Table S2.

(C) Percentages of genotypes from larvae derived from the cross between two heterozygous Cenp-T mutants. The number (n) of analyzed larvae is indicated. The raw data are shown in Table S3.

quantified the intensity of the immunosignals on mitotic chromosomes in control and kinetochore-depleted cells (Figure 3B). Depletion of CENP-I, CENP-M, and CENP-N significantly impaired CENP-T localization to mitotic chromatin. In contrast, in cells depleted for outer kinetochore components (Dsn1, Mis12, Nsl1, Spc24, and Spc25), the CENP-T immunosignal could still be observed (Figures 3B and 3C). In addition, depletion of any CCAN component resulted in loss of Dsn1. In contrast, recruitment of Spc24/Spc25, although reduced upon other CCAN depletion, was only completely abolished upon depletion of CENP-I (Figures 3B and 3C), consistent with its severe chromosome alignment defects (Figure 2). Dsn1 and Spc24/Spc25 localization was also abolished in cells depleted of other members of their respective complexes (Figures 3B and 3C; Figure S6). These data suggest that, in *B. mori*, recruitment of CENP-T is dependent on other inner kinetochore components. In turn, CENP-T appears to be required to recruit the Mis12 complex.

Targeting CENP-T to Ectopic Sites Recruits the Ndc80 and Mis12 Outer Kinetochore Complexes

Our next aim was to evaluate whether CENP-T is sufficient to recruit outer kinetochore components. For this, we used *B. mori* cells transfected with a plasmid containing Lac operator (LacO) arrays, which enables targeting of transiently expressed CENP-T-GFP-LacI protein or control (LacI-GFP) constructs to these loci. To test for the presence of kinetochore components, we stained the cells with our custom-made antibodies against the N terminus of CENP-T, Dsn1, and Spc24/Spc25. We selected equal-sized areas over the GFP foci and over mitotic chromosomes and calculated the ratio of their immunosignals to determine recruitment of kinetochore proteins to the LacO array.

As expected, we observed elevated CENP-T immunosignals over the GFP foci compared to endogenous loci in cells expressing full-length *B. mori* CENP-T-GFP-LacI. In addition, we also observed elevated Dsn1 and Spc24/Spc25 immunosignals over the GFP foci, indicating that CENP-T is capable of recruiting both the Mis12 and Ndc80 outer kinetochore complexes. In contrast, in cells expressing LacI-GFP, neither CENP-T, Dsn1, nor Spc24/Spc25 immunosignals are enriched over the LacI-GFP foci (Figure 4).

In cells expressing the DN-CENP-T-GFP-LacI fusion protein that is unable to be recognized by our CENP-T antibody (Figure S5E), we did not measure elevated CENP-T immunosignals over the GFP foci, indicating that endogenous CENP-T is not recruited to the LacO array. The ratios of Dsn1 and Spc24/Spc25 immunosignals were reduced compared to those in cells expressing the full-length CENP-T fusion proteins, which indicates that the N terminus of CENP-T contributes to the recruitment of these outer kinetochore complexes (Figure 4). Given this, we conclude that CENP-T is sufficient for the recruitment of the Ndc80 and Mis12 outer kinetochore complexes and that its N terminus appears to be important for this activity.

CENP-T Is Essential *In Vivo*

We next aimed to evaluate the importance of CENP-T *in vivo*. For this, CRISPR/Cas9-mediated gene editing was applied to introduce mutations into the endogenous CENP-T gene of the *B. mori* N4 reference strain. A mutant (+7) was isolated that contains a 7-bp insertion within the guide RNA target site, causing a premature stop codon in the CENP-T gene (Figure 5A). Because the C terminus of *B. mori* CENP-T containing the HFD and CENP-T extension appears to be essential for its function (Figure S4), the premature stop codon leads to a nonfunctional protein product. Heterozygous CENP-T mutants can be readily propagated, but when crossed to each other, the proportion of unhatched eggs increased to about 30% compared with control crosses (Figure 5B). Genotypic analyses of the progeny of this cross coming from 70% of eggs that hatched did not reveal any homozygous CENP-T mutants (Figure 5C). These results show that, as *in vitro*, CENP-T is also essential for *B. mori in vivo*.

Homologs of CENP-T Are Retained in Independently Derived CenH3-Deficient Insects

Having characterized the function and importance of CENP-T for CenH3-independent kinetochore formation in Lepidoptera, we next profiled its conservation across other CenH3-deficient and CenH3-encoding insects. Orthologs of the lepidopteran CENP-T protein can be readily identified using BLASTP in all CenH3-deficient insects analyzed as well as several

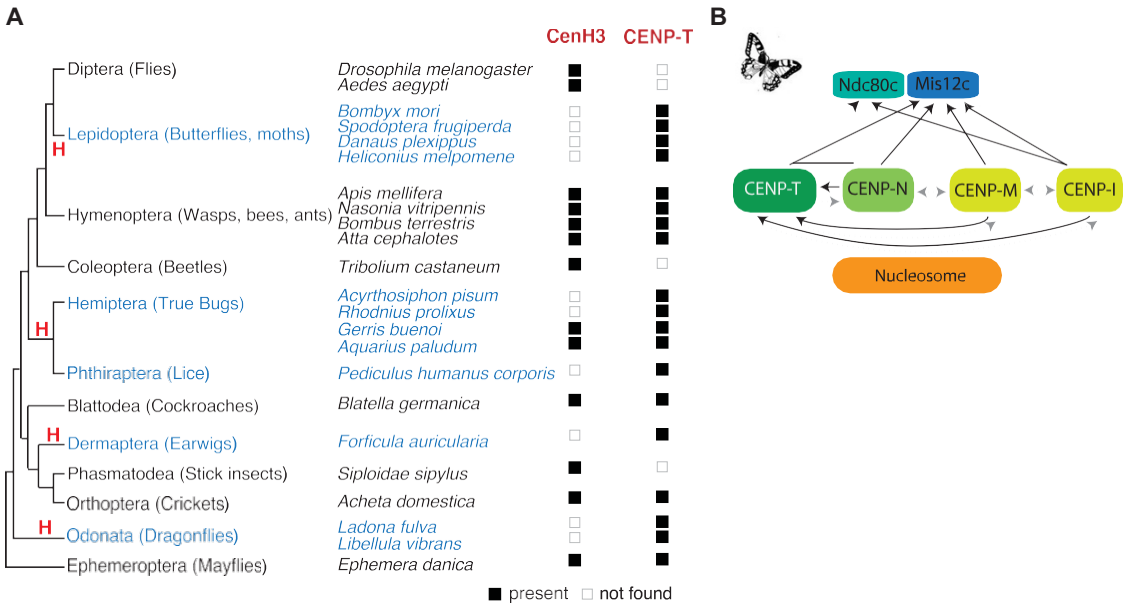

Figure 6. Homologs of CENP-T Are Present in All Other CenH3-Deficient Insects

(A) Holocentric insect orders and species are indicated in blue, and inferred multiple transitions to holocentric chromosomes are labeled with "H." Using protein homology searches of genomes or assembled transcriptomes, the ability and inability to find CenH3 and CENP-T homologs are indicated by a black or white box, respectively. Orthologs of insect CENP-T sequences are listed in Table S1. A phylogeny of a set of HFD sequences from various families, including CENP-T, is shown in Figure S2D, based on HFD sequences listed in Data S2. Although our previous studies did not identify any holocentric insect species that encode for CenH3 [29], searches in additional organisms revealed the presence of putative CenH3 proteins in water striders (Hemiptera). This result provides new insights into the transition to CenH3-deficient holocentric architectures in that the change in centromeric architecture appears to precede the loss of CenH3, perhaps by providing the necessary conditions to allow loss of this otherwise essential component.

(B) Schematic of lepidopteran kinetochore subunits analyzed in this study. Black arrows indicate full localization dependencies. Grey dashed arrows indicate that localization dependency is unknown.

CenH3-encoding insects (Figure 6; Table S1). Notably, phylogenetic analyses of HFD proteins belonging to various HFD families, including CENP-T, indicated accelerated rates of CENP-T protein sequence evolution ancestral to all insects (Figure S2D). Importantly, the retention of CENP-T homologs in independently derived CenH3-deficient insects orders indicates important roles of CENP-T in kinetochores in these organisms.

DISCUSSION

This study provides new insights into the plasticity of kinetochore formation. CenH3 has long been thought to be the cornerstone of kinetochore formation by mediating the attachment of the kinetochore to chromatin. Its direct DNA binding partner CENP-C, in turn, contributes to the assembly of other CCAN components and recruitment of the outer kinetochore in mitosis [5–7, 20, 21, 37]. In addition to these two central components, CENP-T emerged as another core component of the kinetochore, capable of bridging chromatin to the outer kinetochore complex in vertebrates and fungi [8, 9, 24]. Here the discovery and characterization of CENP-T in addition to analyses of other CCAN components in CenH3-deficient Lepidoptera provides first insights into alternative pathways to build a CCAN-based inner kinetochore in a CenH3-independent manner.

Our assays using CENP-T artificial tethering indicate that the role of the lepidopteran CENP-T in outer kinetochore recruitment might be similar to that in vertebrates and fungi. In vertebrates, CENP-T is sufficient for recruitment of both the Mis12 and the Ndc80 complexes by directly interacting with their respective subunits [5, 11, 38]. In fungi, the CENP-T N terminus directly interacts with the Spc24/Spc25 subunit to recruit the Ndc80 complex [8, 39]. Our results show that the lepidopteran CENP-T is also sufficient to recruit the Mis12 and Ndc80 complexes. Whether CENP-T, in particular its N terminus, makes direct protein interactions with any of the Ndc80 or Mis12 complex subunits remains to be shown. However, CENP-T might not be the only factor recruiting outer kinetochore complexes. In fact, though strongly reduced, Spc24/Spc25 and Dsn1 are still present on DN-CENP-T-GFP-LacI foci, which indicates that their recruitment is either aided by more internal regions of CENP-T or via another kinetochore components recruited by CENP-T. Furthermore, our observation that the recruitment of the Spc24/Spc25 is only reduced but not completely abolished upon CENP-T depletion suggests that at least one additional Ndc80 receptor exists at the kinetochore, perhaps via CENP-I (see below).

In addition, other CCAN components also appear to have essential roles in CenH3-independent kinetochore assembly. For example, we find that, upon depletion of CENP-I, Mis12

and Ndc80 complex recruitment is completely abolished, consistent with CENP-I depletion resulting in the strongest mitotic defects. A role of the lepidopteran CENP-I in recruiting the Ndc80 complex would recapitulate previous observations in other organisms showing that the vertebrate CENP-H/I/K/(M) complex contributes to Ndc80 localization [40], that the C terminus of human CENP-I localizes closely to Ndc80 [41], and that CENP-H/I/K/(M) subunits directly interact with Ndc80 in vertebrates and budding yeast [33, 42]. Given these findings together with our CENP-I depletion analyses, it will be interesting to test whether CENP-I or CENP-I complex members makes direct protein interactions with the Ndc80 complex in Lepidoptera and contributes to its recruitment. Overall, the tools that were generated in this study will facilitate future studies to dissect the contribution of CENP-I, other CCANs, or additional kinetochore components with unknown evolutionary relationships (Figure 1) to CenH3-independent kinetochore assembly and chromatin attachment in Lepidoptera.

Considering the essential roles of CenH3 and CENP-C in all other organisms tested, the recurrent loss of these proteins in several insects indicates that the potential for CenH3/CENP-C-independent kinetochore formation might have already arisen in an early insect ancestor. Such potential could be represented in the form of other kinetochore components that evolved the capability to compensate (partially or completely) for CenH3/CENP-C-dependent roles in kinetochore-chromatin attachment and outer kinetochore recruitment. The retention of CENP-T homologs in independently derived CenH3/CENP-C-deficient insects suggests their important contributions to kinetochore assembly, perhaps by contributing CenH3/CENP-C-mediated functions. Among these, future studies will, in particular, aim to evaluate the contribution of the lepidopteran CENP-T in kinetochore-chromatin attachment. Nevertheless, it is also possible that CenH3/CENP-C-mediated functions have been compensated by other CCAN components. In fact, several other CCAN components, including CENP-I and CENP-N, are also retained in CenH3-deficient insects [29], indicating critical roles in their kinetochore assemblies as well. Notably, given that *D. melanogaster* has lost most CCAN components and solely relies on CenH3 and CENP-C for inner kinetochore assembly, it is unlikely that either protein is dispensable for chromosome segregation in this species.

Our results also exemplify the necessity of experimental data to obtain comprehensive pictures of kinetochore complex composition. The characterization of kinetochore components in additional eukaryotes will enable us to obtain better insights into the sequence divergence of kinetochore homologs. This will allow us to increase the information content of our alignments, improving our homology prediction capabilities.

Finally, our studies of kinetochore composition of CenH3-deficient holocentric lepidopteran species, together with the recent finding of a CenH3-deficient monocentric fungus [28, 43] that encodes for other CCAN components, including CENP-T, show that CCAN-based CenH3-independent kinetochore assemblies are considerably widespread in diverse eukaryotes.

STAR+METHODS

Detailed methods are provided in the online version of this paper and include the following:

- KEY RESOURCES TABLE
- LEAD CONTACT AND MATERIALS AVAILABILITY
- EXPERIMENTAL MODEL AND SUBJECT DETAILS
  - Lepidopteran cell lines and culture conditions
  - Culture conditions of B. mori N4 strain
- METHOD DETAILS
  - Alignments and phylogenetic analyses
  - Homology predictions
  - Plasmid construction
  - Construction of cell lines
  - Protein expression and affinity purification
  - Validation of CENP-T and Dsn1 antibody specificity
  - Validation of B. mori Spc24/25 antibody specificity
  - Affinity co-immunoprecipitations
  - Proteomics and Mass Spectrometry Analysis
  - Immunofluorescence
  - Microscopy
  - RNAi-mediated knock-down
  - RNA blot analyses
  - CRISPR-mediated genome editing in B. mori
- QUANTIFICATION AND STATISTICAL ANALYSIS
- DATA AND CODE AVAILABILITY

SUPPLEMENTAL INFORMATION

Supplemental Information can be found online at https://doi.org/10.1016/j.cub.2019.12.014.

ACKNOWLEDGMENTS

We thank Harmit S. Malik and Steve Henikoff for support during the initial steps of this project; Alexander Schleiffer and Eelco Tromer for helpful discussions regarding protein homology predictions; Alexander Schleiffer for sharing a collection of representative histone fold proteins;, Takahiro Kusakabe for the BmN4-SID1 cell line; Tatsuo Fukagawa for the CENP-T-FLAG DT40 cell line we used for control experiments; Abderrahman Khila for access to water-strider genome sequences; Patricia Le Baccon, Mickaël Garnier, and Solène Hervé for help with microscopic analyses; Ahmed El Marjou and Carlos Kikuti for help and advice regarding protein purification and biochemistry; Carsten Janke for advice regarding microtubule staining; all members of the Fachinetti and Drinnenberg labs for helpful discussions; and Leah Rosin and all members of the Drinnenberg lab for input on the manuscript. N.C.-S. receives salary support from Sorbonne Université (2781/2017). This work was supported by "Région Ile-de-France" and Fondation pour la Recherche Médicale grants (to D.L.). This work was supported by grants from JSPS KAKENHI (15H02482 to S.K. and T.K.). I.A.D. and I.L. receive salary support from the CNRS. This work was supported by LabEx DEEP (ANR-11-LABX-0044, ANR-10-IDEX-0001-02), an ATIP-AVENIR research grant, Institut Curie, and the ERC (CENEVO-758757).

AUTHOR CONTRIBUTIONS

N.C.-S. performed and analyzed the cell biological experiments. J.U. and E.H. generated cell lines and performed the IP experiments. T.K. generated and analyzed the *B. mori* CENP-T knockout strain. S.K. supervised the *in vivo* analyses. I.A.D. performed the computational and phylogenetic analyses. G.C. and I.L. generated constructs and helped with the biochemical and cell biological experiments. F.D. carried out the MS experimental work. D.L.

supervised MS and data analysis. I.A.D. supervised the study and secured funding. N.C.-S. and I.A.D. wrote the manuscript.

DECLARATION OF INTERESTS

The authors declare no competing interests.

Received: November 2, 2019
Revised: December 3, 2019
Accepted: December 5, 2019
Published: February 6, 2020

REFERENCES

1. Allshire, R.C., and Karpen, G.H. (2008). Epigenetic regulation of centromeric chromatin: old dogs, new tricks? Nat. Rev. Genet. *9*, 923–937.
2. Fukagawa, T., and Earnshaw, W.C. (2014). The centromere: chromatin foundation for the kinetochore machinery. Dev. Cell *30*, 496–508.
3. Musacchio, A., and Desai, A. (2017). A Molecular View of Kinetochore Assembly and Function. Biology (Basel) *6*, E5.
4. Milks, K.J., Moree, B., and Straight, A.F. (2009). Dissection of CENP-C-directed centromere and kinetochore assembly. Mol. Biol. Cell *20*, 4246–4255.
5. Gascoigne, K.E., Takeuchi, K., Suzuki, A., Hori, T., Fukagawa, T., and Cheeseman, I.M. (2011). Induced ectopic kinetochore assembly bypasses the requirement for CENP-A nucleosomes. Cell *145*, 410–422.
6. Przewloka, M.R., Venkei, Z., Bolanos-Garcia, V.M., Debski, J., Dadlez, M., and Glover, D.M. (2011). CENP-C is a structural platform for kinetochore assembly. Curr. Biol. *21*, 399–405.
7. Screpanti, E., De Antoni, A., Alushin, G.M., Petrovic, A., Melis, T., Nogales, E., and Musacchio, A. (2011). Direct binding of Cenp-C to the Mis12 complex joins the inner and outer kinetochore. Curr. Biol. *21*, 391–398.
8. Schleiffer, A., Maier, M., Litos, G., Lampert, F., Hornung, P., Mechtler, K., and Westermann, S. (2012). CENP-T proteins are conserved centromere receptors of the Ndc80 complex. Nat. Cell Biol. *14*, 604–613.
9. Nishino, T., Rago, F., Hori, T., Tomii, K., Cheeseman, I.M., and Fukagawa, T. (2013). CENP-T provides a structural platform for outer kinetochore assembly. EMBO J. *32*, 424–436.
10. Rago, F., Gascoigne, K.E., and Cheeseman, I.M. (2015). Distinct organization and regulation of the outer kinetochore KMN network downstream of CENP-C and CENP-T. Curr. Biol. *25*, 671–677.
11. Huis In 't Veld, P.J., Jeganathan, S., Petrovic, A., Singh, P., John, J., Krenn, V., Weissmann, F., Bange, T., and Musacchio, A. (2016). Molecular basis of outer kinetochore assembly on CENP-T. eLife *5*, e21007.
12. Monda, J.K., and Cheeseman, I.M. (2018). The kinetochore-microtubule interface at a glance. J. Cell Sci. *131*, jcs214577.
13. Earnshaw, W.C., and Rothfield, N. (1985). Identification of a family of human centromere proteins using autoimmune sera from patients with scleroderma. Chromosoma *91*, 313–321.
14. Palmer, D.K., O'Day, K., Trong, H.L., Charbonneau, H., and Margolis, R.L. (1991). Purification of the centromere-specific protein CENP-A and demonstration that it is a distinctive histone. Proc. Natl. Acad. Sci. USA *88*, 3734–3738.
15. Sullivan, K.F., Hechenberger, M., and Masri, K. (1994). Human CENP-A contains a histone H3 related histone fold domain that is required for targeting to the centromere. J. Cell Biol. *127*, 581–592.
16. Howman, E.V., Fowler, K.J., Newson, A.J., Redward, S., MacDonald, A.C., Kalitsis, P., and Choo, K.H. (2000). Early disruption of centromeric chromatin organization in centromere protein A (Cenpa) null mice. Proc. Natl. Acad. Sci. USA *97*, 1148–1153.
17. Yoda, K., Ando, S., Morishita, S., Houmura, K., Hashimoto, K., Takeyasu, K., and Okazaki, T. (2000). Human centromere protein A (CENP-A) can replace histone H3 in nucleosome reconstitution in vitro. Proc. Natl. Acad. Sci. USA *97*, 7266–7271.
18. Heun, P., Erhardt, S., Blower, M.D., Weiss, S., Skora, A.D., and Karpen, G.H. (2006). Mislocalization of the *Drosophila* centromere-specific histone CID promotes formation of functional ectopic kinetochores. Dev. Cell *10*, 303–315.
19. Carroll, C.W., Silva, M.C.C., Godek, K.M., Jansen, L.E.T., and Straight, A.F. (2009). Centromere assembly requires the direct recognition of CENP-A nucleosomes by CENP-N. Nat. Cell Biol. *11*, 896–902.
20. Carroll, C.W., Milks, K.J., and Straight, A.F. (2010). Dual recognition of CENP-A nucleosomes is required for centromere assembly. J. Cell Biol. *189*, 1143–1155.
21. Kato, H., Jiang, J., Zhou, B.-R., Rozendaal, M., Feng, H., Ghirlando, R., Xiao, T.S., Straight, A.F., and Bai, Y. (2013). A conserved mechanism for centromeric nucleosome recognition by centromere protein CENP-C. Science *340*, 1110–1113.
22. Falk, S.J., Guo, L.Y., Sekulic, N., Smoak, E.M., Mani, T., Logsdon, G.A., Gupta, K., Jansen, L.E.T., Van Duyne, G.D., Vinogradov, S.A., et al. (2015). Chromosomes. CENP-C reshapes and stabilizes CENP-A nucleosomes at the centromere. Science *348*, 699–703.
23. Sugimoto, K., Yata, H., Muro, Y., and Himeno, M. (1994). Human centromere protein C (CENP-C) is a DNA-binding protein which possesses a novel DNA-binding motif. J. Biochem. *116*, 877–881.
24. Hori, T., Amano, M., Suzuki, A., Backer, C.B., Welburn, J.P., Dong, Y., McEwen, B.F., Shang, W.-H., Suzuki, E., Okawa, K., et al. (2008). CCAN makes multiple contacts with centromeric DNA to provide distinct pathways to the outer kinetochore. Cell *135*, 1039–1052.
25. Nishino, T., Takeuchi, K., Gascoigne, K.E., Suzuki, A., Hori, T., Oyama, T., Morikawa, K., Cheeseman, I.M., and Fukagawa, T. (2012). CENP-T-W-S-X forms a unique centromeric chromatin structure with a histone-like fold. Cell *148*, 487–501.
26. Talbert, P.B., Bayes, J.J., and Henikoff, S. (2009). Evolution of Centromeres and Kinetochores: A Two-Part Fugue. In The Kinetochore, P. De Wulf, and W.C. Earnshaw, eds. (New York, NY: Springer New York), pp. 1–37.
27. Akiyoshi, B., and Gull, K. (2014). Discovery of unconventional kinetochores in kinetoplastids. Cell *156*, 1247–1258.
28. Navarro-Mendoza, M.I., Pérez-Arques, C., Panchal, S., Nicolás, F.E., Mondo, S.J., Ganguly, P., Pangilinan, J., Grigoriev, I.V., Heitman, J., Sanyal, K., et al. (2019). Early diverging fungus Mucor circinelloides lacks centromeric histone CENP-A and displays a mosaic of point and regional centromeres. Curr. Biol. *29*, 3791–3802.e6.
29. Drinnenberg, I.A., deYoung, D., Henikoff, S., and Malik, H.S. (2014). Recurrent loss of CenH3 is associated with independent transitions to holocentricity in insects. eLife *3*.
30. Drozdetskiy, A., Cole, C., Procter, J., and Barton, G.J. (2015). JPred4: a protein secondary structure prediction server. Nucleic Acids Res. *43* (W1), W389-94.
31. Tromer, E. (2017). Evolution of the Kinetochore Network in Eukaryotes. Doctoral dissertation (Utrecht University).
32. Collins, C.M., Malacrida, B., Burke, C., Kiely, P.A., and Dunleavy, E.M. (2018). ATP synthase F_1 subunits recruited to centromeres by CENP-A are required for male meiosis. Nat. Commun. *9*, 2702.
33. Pekgöz Altunkaya, G., Malvezzi, F., Demianova, Z., Zimniak, T., Litos, G., Weissmann, F., Mechtler, K., Herzog, F., and Westermann, S. (2016). CCAN Assembly Configures Composite Binding Interfaces to Promote Cross-Linking of Ndc80 Complexes at the Kinetochore. Curr. Biol. *26*, 2370–2378.
34. Baudoin, N.C., and Cimini, D. (2018). A guide to classifying mitotic stages and mitotic defects in fixed cells. Chromosoma *127*, 215–227.
35. Mon, H., Lee, J.M., Sato, M., and Kusakabe, T. (2017). Identification and functional analysis of outer kinetochore genes in the holocentric insect Bombyx mori. Insect Biochem. Mol. Biol. *86*, 1–8.

36. Kobayashi, I., Tsukioka, H., Kómoto, N., Uchino, K., Sezutsu, H., Tamura, T., Kusakabe, T., and Tomita, S. (2012). SID-1 protein of *Caenorhabditis elegans* mediates uptake of dsRNA into Bombyx cells. Insect Biochem. Mol. Biol. *42*, 148–154.

37. Klare, K., Weir, J.R., Basilico, F., Zimniak, T., Massimiliano, L., Ludwigs, N., Herzog, F., and Musacchio, A. (2015). CENP-C is a blueprint for constitutive centromere-associated network assembly within human kinetochores. J. Cell Biol. *210*, 11–22.

38. Hara, M., Ariyoshi, M., Okumura, E.-I., Hori, T., and Fukagawa, T. (2018). Multiple phosphorylations control recruitment of the KMN network onto kinetochores. Nat. Cell Biol. *20*, 1378–1388.

39. Malvezzi, F., Litos, G., Schleiffer, A., Heuck, A., Mechtler, K., Clausen, T., and Westermann, S. (2013). A structural basis for kinetochore recruitment of the Ndc80 complex via two distinct centromere receptors. EMBO J. *32*, 409–423.

40. Cheeseman, I.M., Hori, T., Fukagawa, T., and Desai, A. (2008). KNL1 and the CENP-H/I/K complex coordinately direct kinetochore assembly in vertebrates. Mol. Biol. Cell *19*, 587–594.

41. Suzuki, A., Badger, B.L., and Salmon, E.D. (2015). A quantitative description of Ndc80 complex linkage to human kinetochores. Nat. Commun. *6*, 8161.

42. Mikami, Y., Hori, T., Kimura, H., and Fukagawa, T. (2005). The functional region of CENP-H interacts with the Nuf2 complex that localizes to centromere during mitosis. Mol. Cell. Biol. *25*, 1958–1970.

43. van Hooff, J.J., Tromer, E., van Wijk, L.M., Snel, B., and Kops, G.J. (2017). Evolutionary dynamics of the kinetochore network in eukaryotes as revealed by comparative genomics. EMBO Rep. *18*, 1559–1571.

44. Truett, G.E., Heeger, P., Mynatt, R.L., Truett, A.A., Walker, J.A., and Warman, M.L. (2000). Preparation of PCR-quality mouse genomic DNA with hot sodium hydroxide and tris (HotSHOT). Biotechniques *29*, 52, 54.

45. Vodala, S., Abruzzi, K.C., and Rosbash, M. (2008). The nuclear exosome and adenylation regulate posttranscriptional tethering of yeast GAL genes to the nuclear periphery. Mol. Cell *31*, 104–113.

46. Prendergast, L., Müller, S., Liu, Y., Huang, H., Dingli, F., Loew, D., Vassias, I., Patel, D.J., Sullivan, K.F., and Almouzni, G. (2016). The CENP-T/-W complex is a binding partner of the histone chaperone FACT. Genes Dev. *30*, 1313–1326.

47. Muller, H., Annaluru, N., Schwerzmann, J.W., Richardson, S.M., Dymond, J.S., Cooper, E.M., Bader, J.S., Boeke, J.D., and Chandrasegaran, S. (2012). Assembling large DNA segments in yeast. Methods Mol. Biol. *852*, 133–150.

48. Katoh, K., and Standley, D.M. (2013). MAFFT multiple sequence alignment software version 7: improvements in performance and usability. Mol. Biol. Evol. *30*, 772–780.

49. Waterhouse, A.M., Procter, J.B., Martin, D.M.A., Clamp, M., and Barton, G.J. (2009). Jalview Version 2–a multiple sequence alignment editor and analysis workbench. Bioinformatics *25*, 1189–1191.

50. Guindon, S., Dufayard, J.-F., Lefort, V., Anisimova, M., Hordijk, W., and Gascuel, O. (2010). New algorithms and methods to estimate maximum-likelihood phylogenies: assessing the performance of PhyML 3.0. Syst. Biol. *59*, 307–321.

51. Letunic, I., and Bork, P. (2019). Interactive Tree Of Life (iTOL) v4: recent updates and new developments. Nucleic Acids Res. *47* (W1), W256–W259.

52. Harrison, P.M. (2017). fLPS: Fast discovery of compositional biases for the protein universe. BMC Bioinformatics *18*, 476.

53. Potter, S.C., Luciani, A., Eddy, S.R., Park, Y., Lopez, R., and Finn, R.D. (2018). HMMER web server: 2018 update. Nucleic Acids Res. *46* (W1), W200–W204.

54. Zimmermann, L., Stephens, A., Nam, S.-Z., Rau, D., Kübler, J., Lozajic, M., Gabler, F., Söding, J., Lupas, A.N., and Alva, V. (2018). A Completely Reimplemented MPI Bioinformatics Toolkit with a New HHpred Server at its Core. J. Mol. Biol. *430*, 2237–2243.

55. Kelley, L.A., Mezulis, S., Yates, C.M., Wass, M.N., and Sternberg, M.J.E. (2015). The Phyre2 web portal for protein modeling, prediction and analysis. Nat. Protoc. *10*, 845–858.

56. Poullet, P., Carpentier, S., and Barillot, E. (2007). myProMS, a web server for management and validation of mass spectrometry-based proteomic data. Proteomics *7*, 2553–2556.

57. Schindelin, J., Arganda-Carreras, I., Frise, E., Kaynig, V., Longair, M., Pietzsch, T., Preibisch, S., Rueden, C., Saalfeld, S., Schmid, B., et al. (2012). Fiji: an open-source platform for biological-image analysis. Nat. Methods *9*, 676–682.

58. Naito, Y., Hino, K., Bono, H., and Ui-Tei, K. (2015). CRISPRdirect: software for designing CRISPR/Cas guide RNA with reduced off-target sites. Bioinformatics *31*, 1120–1123.

59. Gouin, A., Bretaudeau, A., Nam, K., Gimenez, S., Aury, J.-M., Duvic, B., Hilliou, F., Durand, N., Montagné, N., Darboux, I., et al. (2017). Two genomes of highly polyphagous lepidopteran pests (Spodoptera frugiperda, Noctuidae) with different host-plant ranges. Sci. Rep. *7*, 11816.

60. Nègre, V., Hôtelier, T., Volkoff, A.-N., Gimenez, S., Cousserans, F., Mita, K., Sabau, X., Rocher, J., López-Ferber, M., d'Alençon, E., et al. (2006). SPODOBASE: an EST database for the lepidopteran crop pest Spodoptera. BMC Bioinformatics *7*, 322.

61. Kawamoto, M., Jouraku, A., Toyoda, A., Yokoi, K., Minakuchi, Y., Katsuma, S., Fujiyama, A., Kiuchi, T., Yamamoto, K., and Shimada, T. (2019). High-quality genome assembly of the silkworm, Bombyx mori. Insect Biochem. Mol. Biol. *107*, 53–62.

62. Madeira, F., Park, Y.M., Lee, J., Buso, N., Gur, T., Madhusoodanan, N., Basutkar, P., Tivey, A.R.N., Potter, S.C., Finn, R.D., and Lopez, R. (2019). The EMBL-EBI search and sequence analysis tools APIs in 2019. Nucleic Acids Res. *47* (W1), W636–W641.

63. Lemoine, F., Correia, D., Lefort, V., Doppelt-Azeroual, O., Mareuil, F., Cohen-Boulakia, S., and Gascuel, O. (2019). NGPhylogeny.fr: new generation phylogenetic services for non-specialists. Nucleic Acids Res. *47* (W1), W260–W265.

64. Lefort, V., Longueville, J.-E., and Gascuel, O. (2017). SMS: Smart Model Selection in PhyML. Mol. Biol. Evol. *34*, 2422–2424.

65. Sayers, E.W., Beck, J., Brister, J.R., Bolton, E.E., Canese, K., Comeau, D.C., Funk, K., Ketter, A., Kim, S., Kimchi, A., et al. (2019). Database resources of the National Center for Biotechnology Information. Nucleic Acids Res. *47*, D23–D28.

66. Jones, D.T. (1999). Protein secondary structure prediction based on position-specific scoring matrices. J. Mol. Biol. *292*, 195–202.

67. Gruber, M., Söding, J., and Lupas, A.N. (2006). Comparative analysis of coiled-coil prediction methods. J. Struct. Biol. *155*, 140–145.

68. Hinshaw, S.M., and Harrison, S.C. (2019). The structure of the Ctf19c/CCAN from budding yeast. eLife *8*, e44239.

69. Schmitzberger, F., and Harrison, S.C. (2012). RWD domain: a recurring module in kinetochore architecture shown by a Ctf19-Mcm21 complex structure. EMBO Rep. *13*, 216–222.

70. Hu, L., Huang, H., Hei, M., Yang, Y., Li, S., Liu, Y., Dou, Z., Wu, M., Li, J., Wang, G.-Z., et al. (2019). Structural analysis of fungal CENP-H/I/K homologs reveals a conserved assembly mechanism underlying proper chromosome alignment. Nucleic Acids Res. *47*, 468–479.

71. Hartlepp, K.F., Fernández-Tornero, C., Eberharter, A., Grüne, T., Müller, C.W., and Becker, P.B. (2005). The histone fold subunits of *Drosophila* CHRAC facilitate nucleosome sliding through dynamic DNA interactions. Mol. Cell. Biol. *25*, 9886–9896.

72. Petrovic, A., Keller, J., Liu, Y., Overlack, K., John, J., Dimitrova, Y.N., Jenni, S., van Gerwen, S., Stege, P., Wohlgemuth, S., et al. (2016). Structure of the MIS12 Complex and Molecular Basis of Its Interaction with CENP-C at Human Kinetochores. Cell *167*, 1028–1040.e15.

73. Armisén, D., Rajakumar, R., Friedrich, M., Benoit, J.B., Robertson, H.M., Panfilio, K.A., Ahn, S.-J., Poelchau, M.F., Chao, H., Dinh, H., et al. (2018). The genome of the water strider Gerris buenoi reveals expansions

of gene repertoires associated with adaptations to life on the water. BMC Genomics *19*, 832.

74. Gibson, D.G. (2011). Gene and genome construction in yeast. Curr. Protoc. Mol. Biol., Chapter 3, Unit 3.22.
75. Gibson, D.G., Young, L., Chuang, R.-Y., Venter, J.C., Hutchison, C.A., 3rd, and Smith, H.O. (2009). Enzymatic assembly of DNA molecules up to several hundred kilobases. Nat. Methods *6*, 343–345.
76. Skene, P.J., and Henikoff, S. (2015). A simple method for generating high-resolution maps of genome-wide protein binding. eLife *4*, e09225.
77. Bosch Grau, M., Gonzalez Curto, G., Rocha, C., Magiera, M.M., Marques Sousa, P., Giordano, T., Spassky, N., and Janke, C. (2013). Tubulin glycylases and glutamylases have distinct functions in stabilization and motility of ependymal cilia. J. Cell Biol. *202*, 441–451.
78. Bassett, A.R., Tibbit, C., Ponting, C.P., and Liu, J.-L. (2013). Highly efficient targeted mutagenesis of *Drosophila* with the CRISPR/Cas9 system. Cell Rep. *4*, 220–228.
79. Yamaguchi, J., Mizoguchi, T., and Fujiwara, H. (2011). siRNAs induce efficient RNAi response in Bombyx mori embryos. PLoS ONE *6*, e25469.
80. Ota, S., Hisano, Y., Muraki, M., Hoshijima, K., Dahlem, T.J., Grunwald, D.J., Okada, Y., and Kawahara, A. (2013). Efficient identification of TALEN-mediated genome modifications using heteroduplex mobility assays. Genes Cells *18*, 450–458.
81. Ansai, S., Inohaya, K., Yoshiura, Y., Schartl, M., Uemura, N., Takahashi, R., and Kinoshita, M. (2014). Design, evaluation, and screening methods for efficient targeted mutagenesis with transcription activator-like effector nucleases in medaka. Dev. Growth Differ. *56*, 98–107.
82. Vizcaı´no, J.A., Csordas, A., Del-Toro, N., Dianes, J.A., Griss, J., Lavidas, I., Mayer, G., Perez-Riverol, Y., Reisinger, F., Ternent, T., et al. (2016). 2016 update of the PRIDE database and its related tools. Nucleic Acids Res. *44*, 11033.

STAR+METHODS

KEY RESOURCES TABLE

REAGENT or RESOURCE	SOURCE	IDENTIFIER
Antibodies		
Mouse monoclonal Anti-FLAG M2 antibody	Sigma	Cat#F1804; RRID: AB_262044
Rabbit polyclonal anti-Spc24/25 (rabbit 1621016)	This study	N/A
Rabbit polyclonal anti-CENP-T (rabbit 045)	This study	N/A
Rabbit polyclonal anti-Dsn1 (rabbit 1615031)	This study	N/A
Mouse monoclonal anti-6xHis	Sigma	Cat#ab18184; RRID:AB_444306
Goat monoclonal IRDye 680RD anti-Rabbit IgG	LI-COR	Cat#926-68071; RRID:AB_10956166
Donkey monoclonal IRDye 800CW anti-mouse IgG	LI-COR	Cat#926-32212; RRID:AB_621847
Mouse monoclonal anti-FLAG M2 beads	Sigma	Cat#M8823; RRID:AB_2637089
Mouse monoclonal anti-a-tubulin Alexa Fluor 488	Thermo Fisher Scientific	Cat#53-4502-80; RRID:AB_1210526
Mouse monoclonal anti-FLAG M2	Sigma	Cat#F1804; RRID:AB_262044
Rat monoclonal anti-phospho Histone H3-Ser10	Sigma	Cat#MABE939
Goat polyclonal anti-rabbit IgG Alexa Fluor 568	Thermo Fisher Scientific	Cat#A-11011; RRID:AB_143157
Goat polyclonal anti-rat IgG Alexa Fluor 568	Thermo Fisher Scientific	Cat#A-11077; RRID:AB_2534121
Goat polyclonal anti-rat IgG Alexa Fluor 488	Thermo Fisher Scientific	Cat#A-11006; RRID:AB_2534074
Goat polyclonal anti-mouse IgG Alexa Fluor 488	Thermo Fisher Scientific	Cat#A-11029; RRID:AB_2534088
Goat polyclonal anti-mouse IgG Alexa Fluor 568	Thermo Fisher Scientific	Cat#A-11004; RRID:AB_2534072
Goat polyclonal anti-rat IgG Alexa Fluor 633	Thermo Fisher Scientific	Cat#A-21094; RRID:AB_2535749
Bacterial and Virus Strains		
E. coli Bl21DE30 plys pRare	Sigma	71400
B. mori Spc24/Spc25 baculovirus	This study	N/A
DH10BacLL	Ahmed EL-Marjou	N/A
Chemicals, Peptides, and Recombinant Proteins		
Cellfectin II	GIBCO	Cat#10362100
cOmplete Protease Inhibitor Cocktail	Roche	Cat#11697498001
SUMO-Protease	Ahmed EL-Marjou	N/A
Bolt 4-12% Bis-Tris Plus denaturing gels	Invitrogen	Cat#NW04120BOX
MNase	Sigma	Cat#N3755-500UN
FLAG peptide	Sigma	Cat#F4799
Novex 16% Tris Glycine Precast Gels	Invitrogen	Cat#XP00162BOX
Magnetic Dynabeads Protein A	Invitrogen	Cat#10002D
DNase I	Roche	Cat#04716728001
4-20% Tris glycine gels	Invitrogen	Cat#XP04200BOX
Instant*Blue*	Sigma	Cat#ISB1L
PVDF membrane	Bio-Rad	Cat#170-4272
Odyssey Blocking buffer	LI-COR	Cat#927-50000
Trypsin/LysC Mix, Mass Spec Grad	Promega	Cat#v5071
LabSafe GEL Blue	GBiosciences	Cat#786-35
NuPAGE 10% Bis-Tris Protein Gels, 1.0 mm, 10-well	Invitrogen	Cat#NP0301BOX
DTT, dithiothreitol	Euromedex	Cat#EU0006-B
Iodoacetamide	Sigma-Aldrich	Cat#I6125
MeCN, acetonitrile	Merck	Cat#1.00099
HCOOH, formic acid	Fluka	Cat#94318

(*Continued on next page*)

Continued

REAGENT or RESOURCE	SOURCE	IDENTIFIER
NH_4HCO_3, ammonuim bicarbonate	Fluka	Cat#09830
DAPI	Sigma	Cat#D9542
Vectashield Antifade Mounting Medium	Vector Laboratories	Cat# H-1000; RRID:AB_2336789
Dithiobis(succinimidyl propionate, DSP)	Thermo Fisher Scientific	Cat#22585
Hank's balanced salt solution (HBSS)	GIBCO	Cat#14025050
TRIzol	Invitrogen	Cat#15596018
NorthernMax-Gly Sample Loading Dye	Thermo Fisher Scientific	Cat#AM8551
NorthernMax-Gly Gel Running Buffer	Thermo Fisher Scientific	Cat#AM8678
QuickHyb solution	Agilent	Cat#201220
Salmon-sperm ssDNA	Sigma	Cat#31149
Cas9 Nuclease protein NLS	NIPPON GENE	Cat#319-08641
Critical Commercial Assays		
Gateway system	Invitrogen	Cat#11791019
Branson Digital Sonifier SFX550	Branson Ultrasonics	N/A
Protino Ni-TED 1000 columns	Machery-Nagel	Cat#745110.50
Covaris E220 Evolution ultrasonicator	Covaris	N/A
Amicon Ultra-0.5 mL 3K MWCO filters	Sigma	Cat#UFC5003
Pierce Silver Stain Kit	Thermo Fisher Scientific	Cat#24612
C18 precolumn (300 mm inner diameter x 5 mm)	Thermo Fisher Scientific	Cat#164942
C18 column (75 mm inner diameter x 50 cm)	Thermo Fisher Scientific	Cat#164535
Orbitrap Fusion Tribrid mass spectrometer	Thermo Fisher Scientific	N/A
UltiMate 3000 RSLCnano System	Thermo Fisher Scientific	N/A
Nanospay Flex ion source	Thermo Fisher Scientific	N/A
Q Exactive HF-X	Thermo Fisher Scientific	N/A
TurboBlotter System	Bio-Rad	Cat#1704155
MAXIscript T7 Transcription kit	Thermo Fisher Scientific	Cat#AM1312
Tris (HotSHOT) method	[44]	N/A
KOD One	TOYOBO	Cat# KMM-101
MultiNA microchip electrophoresis system	SHIMADZU	N/A
MultiNA microchip electrophoresis system - DNA-500 reagent kit	SHIMADZU	Cat# 292-27910-91
BigDye Terminator v3.1 Cycle Sequencing Kit	Applied Biosystems	Cat#4337454
ABI PRISM 3130xl Genetic Analyzer	Applied Biosystems	N/A
Deposited Data		
Proteomics data	This study	PRIDE: PXD016092
Experimental Models: Cell Lines		
BmN4	ATCC	Cat#CRL-8910; RRID: CVCL_Z633
BmN4-SID1	[36]	RRID:CVCL_Z091
Sf9	GIBCO	Cat#12659017
Sf9-LacO	This study	N/A
Experimental Models: Organisms/Strains		
Non-diapause *B. mori* strain N4	University of Tokyo	N/A
Cenp-T mutant *B. mori*	This study	N/A
Oligonucleotides		
Oligonucleotides are listed in Table S6	This study	N/A
Recombinant DNA		
pIBV5 plasmid	Invitrogen	Cat#12550018
pENTR vector	Invitrogen	Cat#K240020

(*Continued on next page*)

Continued

REAGENT or RESOURCE	SOURCE	IDENTIFIER
pVS1-LacO	[45]	Addgene RRID: Addgene_33143
eGFP_N1_LacI pDEST	Geneviève Almouzni lab [46]	N/A
pCMV-lacI	Geneviève Almouzni lab Agilent	Cat#217450
pRS416	[47]	N/A
pIZV5	Invitrogen	Cat#V800001
pT7-His-SUMO vector	Ahmed EL-Marjou	N/A
pRSF-DUET1	Sigma	Cat#71341
Software and Algorithms		
MAFFT	[48]	https://mafft.cbrc.jp/alignment/software/
Jalview	[49]	https://www.jalview.org/
Jpred4	[30]	http://www.compbio.dundee.ac.uk/jpred/
PhyML 3.0	[50]	http://www.atgc-montpellier.fr/phyml/
iTOL vs4	[51]	http://itol.embl.de
fLPS	[52]	http://biology.mcgill.ca/faculty/harrison/flps.html, or https://github.com/pmharrison/flps
HMMER webserver	[53]	http://www.ebi.ac.uk/Tools/hmmer
HHpred version 3.2.0	[54]	https://toolkit.tuebingen.mpg.de/tools/hhpred
phyre2 predictions	[55]	http://www.sbg.bio.ic.ac.uk/phyre2/html/page.cgi?id=index
Proteome Discoverer (v 2.2)	ThermoFisher Scientific	N/A
myProMS	[56]	https://github.com/bioinfo-pf-curie/myproms
Fiji	[57]	http://fiji.sc/
Prism version 8.12 for Mac	GraphPad Software	https://www.graphpad.com/scientific-software/prism/
CRISPRdirect	[58]	https://crispr.dbcls.jp/
Other		
S. frugiperda ''corn strain'' annotation	[59]	https://bipaa.genouest.org/sp/spodoptera_frugiperda_pub/
S. frugiperda ''rice strain'' annotation	[59]	https://bipaa.genouest.org/sp/spodoptera_frugiperda_pub/
S. frugiperda transcriptome TR2012b	[60]	http://bioweb.ensam.inra.fr/spodobase
SilkBase	[61]	http://silkbase.ab.a.u-tokyo.ac.jp; RRID:SCR_008242

LEAD CONTACT AND MATERIALS AVAILABILITY

All the reagents generated in this study are available for sharing. Further information and requests for resources and reagents should be directed to and will be fulfilled by the Lead Contact, Ines Anna Drinnenberg (ines.drinnenberg@curie.fr).

EXPERIMENTAL MODEL AND SUBJECT DETAILS

Lepidopteran cell lines and culture conditions

Cultured silkworm ovary-derived BmN4 (ATCC Cat#CRL-8910; RRID: CVCL_Z633) and BmN4-SID1 cell lines (RRID:CVCL_Z091) [36] were maintained in Sf-900 II SFM medium (GIBCO Cat#10902-088) supplemented with 10% fetal bovine serum (Eurobio Cat#CVFSVF0001), antibiotic-antimycotic (GIBCO Cat#15240-062) and 2mM L-glutamine (GIBCO Cat#25030-024) at 27°C. Sf9 cells (GIBCO Cat#12659017) were maintained in Sf-900 II SFM medium (GIBCO Cat#10902-088) supplemented with antibiotic-antimycotic (GIBCO Cat#15240-062) and 2mM L-glutamine (GIBCO Cat#25030-024) at 27°C.

Culture conditions of B. mori N4 strain

Non-diapaused larvae of the *B. mori* N4 strain were fed with fresh mulberry leaves or artificial diet SilkMate (NOSAN SilkMate PS) under a continuous cycle of 12-h light and 12-h darkness at 25°C.

METHOD DETAILS

Alignments and phylogenetic analyses

For Figure 1C and Figure S2C, sequences were aligned with MAFFT on the EMBL-EBI web interface [62], and visualized and processed with Jalview [49] (ClustalX coloring scheme). Secondary structures were predicted using Jpred4 [30]. For Figure S2D, histone fold domains were aligned using MAFFT [48, 63]. A maximum likelihood phylogeny was build using PhyML 3.0 [50] with automatic model selection [64], default parameters and 100 bootstrap permutations. The tree was visualized using iTOL vs4 [51]. Sequences used for the phylogeny are listed in Data S2.

Primary sequence analyses of the *B. mori* and *G. gallus* CENP-T (GenBank: NP_001263242.1) for Figure 1C were performed using fLPS [52] with default parameters. The Arginine-rich N-terminal regions are located between amino acid 4 and 32 of the *G. gallus* CENP-T (*E* value $6.0x10^{-7}$); and 20 and 41 of the *B. mori* CENP-T (*E* value $4.7x10^{-5}$). The proline-rich regions are located between amino acid 493 and 521 of the *G. gallus* CENP-T (*E* value $3.4x10^{-8}$); and 850 and 899 of the *B. mori* CENP-T (*E* value $3.7x10^{-4}$).

Homology predictions

The annotation of the *S. frugiperda* corn strain proteome were used for all computational analyses [59]. In case annotations were missing or incorrect we complemented the data using annotations from the *S. frugiperda* ''rice strain'' [59], EST (Transcriptome TR2012b) data [60] or our own analyses. Homologs of *S. frugiperda* proteins identified in the kinetochore IPs were predicted in *B. mori* proteome [61]. Both *S. frugiperda* and *B. mori* proteins were used for homology searches. BLASTP and PSI-BLAST searches were performed in the NCBI non-redundant protein database [65]. Jackhmmer searches were performed on the HMMER webserver [53] against reference proteomes as current as September 2019. HHpred version 3.2.0 searches were performed against the PDB_mmCIF70_3_Aug [54]. Coiled-Coil domains were predicted using PCOILS (window 28) [54, 66, 67].

CENP-T

For iterative HMM profile searches only the C-termini containing the HFD and 2 helix extension of the *B. mori* or *S. frugiperda* proteins were used.

> B_mori_CENPT_CTERM

TTKRLYKYLEDKLEPKYDYKARVRAEKLVETIYHFTKEVKKHEVAPNDAVDVLKHEMARLDIVKTHFDFYQFFHDFMPREIRVKVVPDIVN
KITIPRNGVFSEILSGHAVHA

> S_frugiperda_CENPT_CTERM

ITKRLYKFLETKLEPKYDYKARVRAEKLVETIYHFAKDLRRHDVAPTDAVDVLKHELARLEVVQTHFEFYEFFHEFMPREVRVKVVPDIVN
KIPLPRHGVFSDILRGNNVQG

HHpred searches using the C terminus of the *B. mori* and S. *frugiperda* CENP-T protein identify the C terminus of the *G. gallus* CENP-T with high probability 94.56% and 94.2% respectively (Figure S2). HHpred searches using the full-length protein also identifies the *G. gallus* CENP-T as a best hit though with lower probabilities (51.9% for the *B. mori* and 50% for the *S. frugiperda* protein). In this search, the alignment between the lepidopteran protein and *G. gallus* CENP-T is restricted to their C-termini. A reciprocal HHpred search using the *G. gallus* HFD helix 3 and CENP-T extension identified *B. mori* protein as best hit (Figure S2).

Known vertebrate CENP-T proteins can also be identified as best hits after 2 jackhmmer iterations using the *B. mori* CENP-T C terminus (Figure S2). Additional arthropod CENP-T from the whiteleg shrimp (*Penaeus vannamei*) and the pill woodlouse (*Armadillidium vulgare*) could be predicted after 4 jackhmmer iterations. Finally, phyre2 predictions [55] using the full-length *B. mori* CENP-T protein predicts the known structure of the *G. gallus* CENP-T C terminus with high confidence (91.5%) while low sequence identity of the aligned regions (14%).

Iterative blastp and tblastn searches using lepidopteran CENP-T proteins against select annotated insect proteomes, genome assemblies and assembled transcriptomes revealed additional orthologs of CENP-T proteins in insects (Table S1).

KWMTBOMO14835 and GSSPFG00001205001

BLASTP searches using both proteins against the non-redundant protein database revealed only hits in Lepidoptera. Iterative PSI-BLAST searches and jackhmmer searches using both proteins also revealed no homologous hits in other insect orders. HHpred searches of GSSPFG00001205001 did not reveal any hits with high probability. However, HHpred searches identified similarity between the N terminus of KWMTBOMO14835 and resolved structure of the *S. cerevisiae* Ctf19 protein (CENP-P) [68] as best hit with high probability (93.58%) while only 13% amino acid identity. The aligned region also includes parts of the tandem RWD domains from *S. cerevisiae* Ctf19. The N terminus of KWMTBOMO14835 has predicted coil-coiled regions (PCOILS, window 28). HHpred predictions of the trimmed protein without the coiled-coil region reduced the probability of similarity to Ctf19 to 43.96%, which was also no longer the best hit.

We therefore refrain from assigning homology to Ctf19 without further functional or structural validations and refer to the lepidopteran proteins as coiled-coil RWD-like proteins.

KWMTBOMO09290 and GSSPFG00019785001

Both proteins contain N-terminal coiled-coil domains (PCOILS, window 28). HHpred searches of both proteins without the N-terminal coiled-coil regions revealed similarities to RWD domains of several kinetochore components including the resolved structure of the *G. gallus* Spc24 globular domain [9] and Mcm21 (CENP-O) subunit of the budding yeast Ctf19 complex [68, 69] with high and similar probabilities. Iterative jackhmmer searches of the trimmed *B. mori* protein without the N-terminal coiled-coil region identified hits in Hymenoptera in the second iteration including *Camponotus floridanus* (UniprotKB: E2AEP7, *E* value 0.0017). The third iteration

identified additional hits in the blattodean *Zootermopsis nevadensis* (UniprotKB: A0A067RMY5, *E* value 0.00028), the arthropod *Daphnia magna* (UniprotKB: A0A0P5Q3Q5, *E* value $6.5x10^{-7}$) and predicted known vertebrate CENP-O proteins in *Anabis testudineus* (UniprotKB: A0A3Q1H0S6, *E* value 0.0023 and UniprotKB: A0A3Q1H0T5, *E* value 0.0037). The fourth iteration identified the human CENP-O (*E* value $1.6x10^{-13}$).

Given the similarity to multiple RWD containing kinetochore proteins and the lack of experimental evidence we only refer to the lepidopteran proteins as coiled-coil RWD-like proteins.

KWMTBOMO06154 and GSSPFG00011797001

HHpred searches did not identify high scoring hits for neither one of the two proteins. GSSPFG00011797001 identified the recently resolved structure of the fungus *Thielavia terrestris* CENP-H [70] but not as the best hit and with only 36% probability. Still, given the presence of CENP-I, CENP-M and the putative CENP-K, it will be worthwhile to test if these proteins are part of a lepidopteran CENP-H-I-K-M complex. Hits in other insect orders could not be predicted using psi-blast or jackhmmer.

LOC101741561 and GSSPFG00006732001

The *B. mori* homolog is not part of the most recent annotations [61], we therefore refer to the ID of previous annotations present on NCBI Genebank in Figure 1.

GSSPFG00006732001 is likely misannotated because most other lepidopteran homologous proteins including GenBank: LOC101741561 only align to the C-terminal part of the protein. We derived a new consensus sequence by aligning available TR2012b transcriptome data [60]. The encoded ORF translates into the following protein:

> *S. frugiperda CENP-K*

MSSDRNKETRDAVKREIKEIQARCKHEWNIIDNSPLDAPNIDLEQINEKALCYIEGLGTGIQNSNTPITADDNLLTSQFLKEIRDKTGQVEE
YTAFVRGSIHDIDAEINRLQTLIKITQEAKARPMLNKCEVQPEHVHRAKERFQVMKNELHSLIHSLFPNCDSLIIETMGQLMAEHLNEESN
GYIPVTAETFQIIELLKDMKIVTVNPYNKLEVKLSY

One of the EST that contain the full ORF is Sf2H05447-5-1 that is listed in Figure 1B.

Iterative PSI-BLAST searches using the *B. mori* protein revealed hits in Hymenoptera including *Athalia rosae* (GenBank: LOC105689000, *E* value $5x10^{-5}$) after the 1st iteration. The 2nd iteration revealed hits in Hemiptera including *Bemisia tabaci* (GenBank: LOC109036758, *E* value 0.003), the Blattodean *Zootermopsis nevadensis* (GenBank: LOC110834781, E value $2x10^{-11}$) and the mollusk *Mizuhopecten yessoensis* (centromere protein K-like, *E* value 0.001). The human CENP-K was identified after the 3rd iteration. These analyses are consistent with previous predictions identifying CENP-K in *B. mori* [31].

Jackhmmer searches of a N-terminal truncated version of the *B. mori* protein without a coiled-coil region also revealed a hit in the phthirapteran *Pediculus humanus corporis* after the 3rd iteration (UniprotKB: E0VW71, *E* value $4.1x10^{-9}$).

KWMTBOMO11351 and GSSPFG00010096001

These are orthologs of *Drosophila melanogaster* bellwether, the alpha subunit F0F1 ATP synthase subunit alpha recently been shown to interact with Cid during *Drosophila melanogaster* male meiosis [32]. Orthologs are present across insects and diverse eukaryotes.

KWMTBOMO11557 and GSSPFG00019290001

HHpred searches aligns both proteins to the structure of the CHRAC 14 HFD [71] as best hits but low probabilities (Probability 49.3% for KWMTBOMO11557 and 39.1% for GSSPFG00019290001). Hits in other insect orders could not be predicted using psi-blast. Jackhammer searches of both proteins converged after 2 iterations.

Sf2H06980-5-1 and KWMTBOMO014775

The *S. frugiperda* protein is not part of the *S. frugiperda* corn strain annotations but in the annotations from the closely-related *S. frugiperda* rice strain [59]. We therefore provide the ID from these annotations file. Both *B. mori* and *S. frugiperda* proteins contain C-terminal coil-coiled regions. HHpred searches using only the N-terminal first 65 amino acids identifies the known structure of the human Nsl1 [72]. Though the human Nsl1 was not the best hit for neither one of the two lepidopteran proteins, given the abundance of the protein in the Nnf1 and Dsn1 IPs we refer to it as Nsl1 candidate. These data suggest that as in other eukaryotes, the lepidopteran Mis12 complex contains four instead of only three components as recently described [35].

Hemipteran CenH3

Hemipteran CenH3 fragments in *Gerris buenoi* genome assembly [73] and *Aquarius paludum* assembly (A. Khila, personal communication) could be identified in TBLASTN searches using *D. melanogaster* H3 as queries.

> *Aquarius_paludum_Embryo_Assembly50_c84768)g2_il*

RRRSGVVALREIRHLQKSTNLLIPKLPFMRIVQEILQSYSTEPYRIQSRALEALQEMTEILMVDLFSEAILCCIHAKRKTIMVQDMRLARRIRG

> *Gerris_buenoi_ KZ651887.1*

RRRSGVVALREIRHLQKSTNLLIPKLPFMRIVKEILQSYSTEPYRLQTQALEALQEMTEILMVDLFSEAILCCLHAKRKTIMVQDMRLARRIRG

Plasmid construction

A list of plasmids generated in this study is provided in Table S4. For the kinetochore IPs, full-length ORFs of *S. frugiperda* CENP-M, CENP-N, CENP-I, CENP-T, Dsn1 and Nnf1 fused to 3xFLAG tags were cloned into pIBV5 (Invitrogen Cat#12550018) using the Gateway system (Invitrogen Cat#11791019) from pENTR vectors (Invitrogen Cat#K240020). The genes encoding for *S. frugiperda* CENP-T, CENP-I and CENP-N are not correctly annotated in the current assembly [59] as inferred by aligning the protein products to the *B. mori* homologs. We inferred the correct ORF sequences from EST data and sequencing of the amplified PCR fragments from Sf9 cDNA.

The following are the correct ORF sequences that were used for all experimental analyses:

> *S. frugiperda CENP-I*

MADVDEIIDYIKSLKKGFDKDLFQNKIDELAYAVDTTGILYNDFHTLFKVWLNLSIPITKWVSLGACLVPQNIVEDRTVEYALSWMLSNYED
QSTFSRIGFLLDWLTAAMECECIEMETLDMGYDVFYVSLTYETLTPHAVKLVYTLTKPVDVTRRRVLELLDYARKREAKKNMFRQLXVLL
GLFKSYKPECVPEDIPAISIHAAFKKINPDLLARFKRNQENRNSVRRERHHLTWINPINSDRGRNKKIDPLVPNVEFLNIGSKQYAEKEHQK
NFLDFTDPVSVLQCSVQRSTSRPARIRALLCNVTGVALLAVASHTEQEFLSHDLHHLLNSCFLNISPHSYREKQDLLHRLAVLQHTLMQG
IPVITRFLAQYLPLWNERDYFAEILELVQWVSLDSPDHVTCVLEPLARAYHRAQPIEQCAILRSLNHMYCNLVYASTRKRHHFMGTPPSP
QVYALVLPKVATAISDMCDKELQVNPEQMVVLHSGVQGAAARARGEARGGAAAGALAPRLALALPLLASSAALLDSVAELMILYKKIFTT
AKQTNVITNTDTFEKQMQVLEAYTSDLINCLYSEGALSDRNLGFVFSKLHPQLVEKLGSLMPDVDAKLSIRNSIAFAPYTYIQLDAIDHRD
ADNKLWFNAVIEQEFTNLSRFLKRAVTELRYQ

> *S. frugiperda CENP-T*

MPKTKIPSPARPQGATTPKRKKSRGSRSVCSPALSTASGRLTSLIDQFKEKNMESFALSPLNRRSILNDDTAIEEPRRQSWWKKLKEDS
HEIMEVLEENKVADSGNNAIEELIDIEVLSQEKKEYTLDLPESSDNESINSIVLPQRKLFTQKENKPQKKFGQFSDNRETLAKLHKTNTQG
DKTVNVGTRELFQNAKRSKPIFPAALLNISPNKTAMDKTKENILPEPKVRNIFGNRPANKRKNMFADFVVSESEDEIPELQPRVFGFQKKL
EQRRISSISKGREGSPASSITTDMEMDDWKLLPSSTMVENQLEDIVAGHTPKRARLSKLSEAKESEAGTLQTNTTGDKTKSSNKSIMSKN
KSKSSPDAKDKSLNSSRTTRSMLKNASKLEENTEPKQDTKTQSKISTKDNALDVSLSKATTKQNTSLNKSLRLNKSRTRNSSKLNEEEM
ETDENVVKNAINDATRVISKNASSAAVASKSINEKERTITLKVHDKASETGSNKEEDDNNFVLQYEDEIVEEATDHNQINENKTTKIKNRNTI
VIENDQETDVNESKSNKSIQKEPKQAKTVEESVESQNEQSGNDNIDGNEIEENAIEQNHESHDGEKISRELNEESNNSEGNDERNVTKDN
KDQENDEEINESQENDEEINLSQESNRDEAVLSRVDEENESEVNEESENEDDVNESNESEEQNESQEVEAEVDESEEIEEQNESQEIENE
ANESQEVNEEADDSKVEENASEDEEENQEVENDEEENAEESQEVDNEESQEIENQEEFEVSQESEHEVSQEVENEEENEEENDEGDQE
VEQEEENQSEDDVEDQVEDQSQEIENDEENDEEENEESQEIENDEENVVESEAEVNESQEIEGDQEMDDSDEADRAIASDPEISDQDDN
GADEMEVDDDDDNNEQESENEEETEGNQEESQEEQQEPSAEEIEESPNVTHDTTGRHRQKVLKSPEAILHDKTNQMDSFTAKGRNTS
IRKTKSMIKNLNIRPSLAPQRDSLAFSDGTRDSSAEGSGWDSHRTTRKTLRQTFGKDFTPRKSLRALVMEKSAKRQTEHMDLHSETSKY
PQANSTELAEDSNGHVDDFVESDHEVSRRTRQTTLETYLQKIKQKNLENKVKMEELVRNSLKAPARDTLSLFKVPNKPAPRRLKPTQNK
PRTQVKAITAFGELPTEVIEDMKYKPPKRFQPTNASWITKRLYKFLETKLEPKYDYKARVRAEKLVETIYHFAKDLRRHDVAPTDAVDVLK
HELARLEVVQTHFEFYEFFHEFMPREVRVKVVPDIVNKIPLPRHGVFSDILRGNNVQG

> *S. frugiperda CENP-N*

MPLEVFCVTALPEFGVRWRELSKAVRNARLPMQPASVARVLCRHVSKALTADEIEDIVARLRLKLVATQPRTWHVIRLSEKTTEEPVTLTM
RAVPGRITQALRKSKKTMRPEVQTVLLGDMLYLSIQLVSEHKSGSALYVATPPGEPVALVSSVNMVGLIKATVEGLGYKSYEIADLHGRDI
PSLLRINDRAWNTNADHLAEIPEYAPTPIITETGIDYTYKAYDENYVENILGPNPPKITDLTIKTSKSFFDRSRLDKNINITINIKTEDLAKSLKC
WVSKGAIAPTSDLIKIFHQIKSNKISYTREDD

To express the C terminus of *S. frugiperda* CENP-T a 166 amino acid C-terminal fragment that contains the HFD and CENP-T extension was isolated to generate the *S. frugiperda* CENP-T-HFDextension-FLAG pIBV5 expression clone.

For LacO/LacI tethering assays, pVS1-LacO (Addgene RRID: Addgene_33143 [45]) was modified to insert the blasticidine resistance cassette from pIBV5 into the BamH1 and Sac1 sites. To generate LacI-GFP pIBV5, the LacI-eGFP insert was amplified from eGFP_N1_LacI pDEST (kind gift from Geneviève Almouzni lab, Nuclear Dynamics unit, UMR3664, Institut Curie, Paris, France [46]) and cloned into pENTR and pIBV5. To generate *B. mori* CENP-T-GFP-LacI pIZV5, the full-length coding sequence of *B. mori* CENP-T from *B. mori* CENP-T-FLAG pIZV5, lacI from pCMV-lacI (kind gift from Geneviève Almouzni lab, Agilent Cat#217450) and eGFP from eGFP_N1_LacI pDEST were isolated by PCR and assembled into the shuttle vector pRS416 (kind gift from Heloise Muller, Nuclear Dynamics unit, UMR3664, Institut Curie, Paris, France) using the yeast-based homologous recombination-based DNA assembly, described in detail in elsewhere [47, 74]. Briefly, *S. cerevisiae* BY4742 strains were transformed with the linear DNA fragments and linearized pRS416, colonies were picked to isolate the resulting recombined construct. The constructs were then transformed and amplified in *E. coli*. The *S. frugiperda* CENP-T-GFP-LacI was isolated from this plasmid and cloned into pIZV5 (Invitrogen Cat#V800001) using KpnI and XbaI. To generate the *B. mori* DN-CENP-T(201-1013)-GFP-LacI pIZV5, a truncated *B. mori* CENP-T-GFP-LacI fragment (without the part coding for the first 200 amino acids was isolated PCR and cloned into pIZV5 using BamHI and XhoI sites.

To generate the *B. mori* CENP-T-FLAG pIZV5 construct, the coding sequence of *B. mori* CENP-T was isolated from a BmN4 cDNA library, fused to the 3xFLAG tag by PCR amplification and cloned into pIZV5 using BamHI and XhoI. To generate the *B. mori* CENP-T RNAi-resistant clone (*B. mori* CENP-Tres-FLAG pIZV5), we ordered a Gblocks gene fragment (IDT) to recode an internal sequence of *B. mori* CENP-T from amino acid 221 – 334. A 5^0 fragment of *B. mori* CENP-T that contains the recoded part was then assembled with the 3^0 fragment of *B. mori* CENP-T fused to a 3xFLAG into pRS416 using yeast-based homologous recombination and subsequently cloned into the into the BamHI and XhoI sites of pIZV5. To generate the *B. mori* DN-CENP-Tres-FLAG pIZV5 and *B. mori* DC-CENP-Tres-FLAG pIZV5, *B. mori* CENP-Tres-FLAG pIZV5 was used as a template to isolate 5^0 or 3^0 truncated fragments to clone those into pIZV5 using BamHI and XhoI. The constructs expressed CENP-T without the first 200 or last 112 amino acids, respectively.

To generate protein antigens for antibody production, we purified protein fragment expressed in bacteria. To generate the *S. frugiperda* SUMO-6xHis-CENP-T (1-122) pT7 and *B. mori* SUMO-6xHis-CENP-T (1-218) pT7 bacterial expression constructs the N-terminal domains of *S. frugiperda* (1-222aa) and *B. mori* (1-218aa) CENP-T were cloned into the pT7-His-SUMO vector (gift from Ahmed El-Marjou, recombinant protein platform, Institut Curie) which included N-terminal 6X His and SUMO tags using Gibson Assembly [75].

To generate the *B. mori* 6xHis-Spc24(73-162)-Spc25(70-211) pRSF-DUET1(Sigma Cat#71341) bacterial expression constructs, the globular domain of *B. mori* Spc24 (73-162aa) was cloned with an N-terminal 6X His-tag into the first cassette of the pRSF-Duet1 vector using the BamHI and PstI restriction sites. For dual expression of Spc24 and Spc25, the globular domain of *B. mori* Spc25 (70-211aa) was also cloned into the second cassette of the same pRSF-Duet1 vector using the Nde I and Xho I restriction sites. To generate the *B. mori* 6xHis-Spc24(73-162)-Spc25(70-211) pFASTBac-Dual for the recombinant baculovirus generation to evaluate the Spc24/25 antibody, the Spc24 and Spc25 fragments were cloned into the BamHI and PstI, and KpnI and XhoI sites of pFASTBac-Dual, respectively.

To generate the *B. mori* 6xHis Dsn1(1-100) pRSF-DUET1 and *S. frugiperda* 6xHis Dsn1(1-99) pRSF-DUET1, N-terminal region of *B. mori* (1-100aa) and *S. frugiperda* (1-99aa) Dsn1 cloning into pRSF-Duet1 with N-terminal 6X His-tag BamHI + PstI.

Construction of cell lines

Around 1-5 μg of plasmid DNA was transfected into 10^6 BmN4 or Sf-9 cells using Cellfectin II (GIBCO Cat#10362100) according to the manufactor's instructions. For IF experiments cells were grown on coverslips before transfections. For the generation of stable polyclonal cell lines, antibiotics were added 48 hours after transfection (300 μg/ml Zeocin (GIBCO Cat#R25001) or 40 μg/ml Blasticidin (GIBCO Cat#R21001)). Selection was continued until no viable untransfected cells were observed.

Protein expression and affinity purification

The *E. coli* Bl21DE30 plys pRare (Sigma Cat#71400) was transformed with bacterial expression vectors containing the recombinant genes. Bacterial cultures (4 L) were initially grown at 37°C, 220 rpm and then induced with 0.5 mM IPTG (Euromedex Cat#EU0008-A). Following expression at 37°C for 4 h, cultures were centrifuged at 6000 *xg* for 15 min to pellet the cells. Cell pellets were resuspended in Wash Buffer (20 mM Tris pH 8, 300 mM NaCl, 10 mM $MgCl_2$, 25 mM imidazole). The resuspended pellets were incubated at 4°C on a roller with the addition of one tablet cOmplete Protease Inhibitor Cocktail (Roche Cat#11697498001), Triton X-100 (1% final concentration), and lysozyme (1 mg/mL final concentration). The mixtures were sonicated at 30% amplitude for 8 min total (30 s pulses) in a Branson Digital Sonifier SFX550 (Branson Ultrasonics Corp.). Cell lysates were centrifuged at 30 000 *xg* for 1 h at 4°C. The soluble fraction was removed and passed through 0.45 μm filter units. The lysates were loaded onto Protino Ni-TED 1000 columns (Machery-Nagel Cat#745110.50) that were pre-equilibrated with Wash Buffer. The columns were washed with 2-3 column volumes of Wash Buffer and proteins were eluted with the following buffer (20 mM Tris, 250 mM imidazole, 300 mM NaCl, pH 8.0). The SUMO tags were cleaved from the CENP-T proteins by digesting the eluates at 4°C with SUMO-Protease (enzyme produced by Ahmed El Marjou, recombinant protein facility, Institut Curie) (final concentration 0.6 mg/mL). The eluates were loaded and migrated in Bolt 4%–12% Bis-Tris Plus denaturing gels (Invitrogen Cat#NW04120BOX). The correct-sized bands corresponding to the proteins without the SUMO tag were excised from the gels and sent to Covalab (Villeurbanne, FR) for generation of antibodies in rabbits. For the generation of antibodies against CENP-T and Dsn1, a 1:1 mix of *B. mori* and *S. frugiperda* CENP-T or Dsn1 protein fragments were injected into rabbits. For the generation of the antibody recognizing Spc24 and Spc25 proteins, the isolated *B. mori* Spc24 and Spc25 protein fragments were injected.

Validation of CENP-T and Dsn1 antibody specificity

For each IP experiment, one confluent flask of BmN4 cells was used. Immunoprecipitation was performed as described previously [76] omitting the cross-linking step and with some modifications. Briefly, cells were spun down and washed with PBS with cOmplete Protease Inhibitor Cocktail (Roche Cat#11697498001). Cells were resuspended in 140 mL lysis buffer (1% SDS, 10 mM EDTA, 50 mM Tris-HCl (pH 8.1)) with protease inhibitors and incubated for 10 minutes at 4°C. 1350 mL IP dilution buffer (1% Triton X-100, 2 mM EDTA, 150 mM NaCl, 20 mM Tris-HCl (pH 8.1)) with protease inhibitors and 4.5 mL CaCl2 (1 M) were added and samples were incubated for 2 minutes at 37°C. Chromatin was digested using I UNIT of MNase (Sigma Cat#N3755-500UN) for 15 minutes at 37°C. The reaction was stopped by adding 30 mL EDTA and 60 mL EGTA followed by mild shearing and solubilization step using the Covaris E220 Evolution ultrasonicator (Covaris) (150 s, peak power 75, duty factor 10, cycles/burst 200). Samples were spun down for 5 minutes at 16000 *xg* and the soluble extract was added to 50 mL magnetic Dynabeads Protein A (Invitrogen Cat#10002D) covalently conjugated to 5 mL of rabbit polyclonal anti-CENP-T (this paper) or anti-Dsn1 (this paper) immunoserum or 10 mg anti-FLAG M2 antibody (Sigma Cat#F1804; RRID: AB_262044) as a control. Immunoprecipitation was performed for 15 minutes at room temperature and samples were washed three times in PBS. Samples were digested on beads for MS analyses (Figures S5A and S5B) (see below).

Validation of B. mori Spc24/25 antibody specificity

The 6xHis-Spc24(73-162)-Spc25(70-211) pFASTBac-Dual construct was used to generate recombinant baculovirus DNA. Briefly, pFASTBac-Dual constructs were transformed into DH10bacLL strain to produce and isolate the recombinant baculovirus backbone. Recombinant baculoviruses were amplified in Sf9 cells to the generate high-titer virus stocks of *B. mori* Spc24/Spc25 baculovirus. 500 ml of the recombinant Spc24/Spc25 expressing baculovirus stock (MOI 100) were used to infect 50ml Sf9 cells (10^6 cells/ml) for 3 days. To obtain total cell extracts, the cell pellet was resuspended in buffer A (20 mM Tris pH 8, 300 mM NaCl, 5% glycerol, one tablet cOmplete Protease Inhibitor Cocktail (Roche Cat#11697498001) and 20ml DNase I (Roche Cat#04716728001)) and incubated for 20 min at 4°C. The samples were sonicated at 20% amplitude for 3 min and 30 s total (30 s pulses) in a Branson Digital Sonifier SFX550 (Branson Ultrasonics Corp.) and centrifugated for 30min at 8000 rpm, at 4°C. The supernatant was used for the subsequent experiments. The lysates were loaded onto Protino Ni-TED 1000 columns (Machery-Nagel) that were pre-equilibrated with Wash

Buffer. After a 30 min incubation at 4°C, the columns were washed in Wash Buffer with 20 mM imidazole followed by several elution steps with increasing concentrations of imidazole (50 mM, 100 mM, 200 mM and 500 mM). Proteins were separated on 4%–20% Tris glycine gels (Invitrogen Cat#XP04200BOX) and visualized using Instant*Blue* (Sigma Cat#ISB1L).

For protein blot analysis, samples were separated on Bolt 4%–12% Bis-Tris Plus gels (Invitrogen Cat#NW04120BOX) and transferred to a PVDF membrane (Bio-Rad Cat#170-4272) using the Trans-Blot Turbo Transfer System (1.3 A, 25 V, 10min). The membrane was blocked using the Odyssey Blocking buffer (LI-COR Cat#927-50000) before primary antibody incubation (rabbit polyclonal anti-Spc24/Spc25 (this paper), 1:1000 dilution and mouse monoclonal anti-6xHis, 1:1000 dilution (Sigma Cat#ab18184; RRID:AB_444306)) and secondary antibody incubation (IRDye 680RD Goat anti-Rabbit IgG (LI-COR Cat#926-68071; RRID:AB_10956166), IRDye 800CW donkey anti-mouse IgG (LI-COR Cat#926-32212; RRID:AB_621847), dilution 1:10000). The signals were visualized on an Odyssey LI-COR scanner (Figure S5C).

Affinity co-immunoprecipitations

Cultures of the following Sf9 strains expressing full length or partial *S. frugiperda* kinetochore proteins fused to a C-terminal or N-terminal 3XFLAG tags or control wild-type Sf9 cells were grown to exponential phase in Sf-900 II SFM medium (GIBCO Cat#10902-088): CENP-I, CENP-M, CENP-N, CENP-T, CENP-T-HFDextension, Dsn I and Nnf1. For each strain, 3 3 10^9 cells were harvested by centrifuging for 10 min at 300 *xg*, and the pellets were washed twice in cold PBS. The pellets were resuspended in 5 mL HDG150 Buffer (20 mM HEPES pH 7.0, 150 mM KCl, 10% glycerol, 0.5 mM DTT, 1 tablet cOmplete Protease Inhibitor), and then cells were disrupted with 50 strokes in a dounce homogenizer at 4°C. The dounced fraction was centrifuged at 1700 *xg* for 10 min at 4°C, and the nuclei (lower fraction) were gently resuspended with 5 mL HDG150 Buffer and re-centrifuged in the same conditions. The nuclei were resuspended in a final volume of 5 mL using HDG150 Buffer. Nuclear extracts were prepared by passing the nuclear fraction 10 times through a 20G 1 1/2'' needle (0.9 3 38 mm) and then 5 times through a 25G 3/8'' needle (0.5 3 16 mm). The nuclear extracts were centrifuged at 20 000 *xg* for 10 min at 4°C in microcentrifuge tubes. The pellets were resuspended in HDG150 Buffer and pooled together at a final volume of 5 mL. To prepare the chromatin, the nuclear extracts were digested with ~40 units MNase (Sigma Cat#N3755-500UN) for 1 hour at 4°C on a roller, 3 mM $CaCl_2$ was added to the digestions. The MNase digestions were stopped by adding 250 mL of 0.2 M EGTA. To solubilize the digested chromatin, 10 mL of HDG400 Buffer (20 mM HEPES pH 7.0, 400 mM KCl, 10% glycerol, 1 mM DTT, 0.05% NP-40, 1 tablet cOmplete Protease Inhibitor) was added to the samples and incubated for 2 h at 4°C on a roller. The samples were centrifuged at 8000 *xg* for 10 min at 4°C. The supernatants were saved to bind to the anti-FLAG M2 beads (Sigma Cat#M8823; RRID:AB_2637089). The M2 magnetic beads were prepared according to the manufacturer's recommendations. The digested chromatin samples were incubated with 150 mL anti-FLAG M2 beads. The beads were washed four times with 1 mL HDGN320 Buffer (20 mM HEPES pH 7.0, 320 mM KCl, 10% glycerol, 1 mM DTT, 0.05% NP-40, 1 tablet cOmplete Protease Inhibitor). For proteomic analyses of full-length kinetochore protein IPs, beads were boiled in sample buffer to first run those into gels (see below). For proteomic analyses of the CENP-T-HFDextension IP, proteins were directly digested on beads (see below). For the silver stainings of Sf9 kinetochore IP samples shown in Figure S1, M2 beads were incubated with FLAG peptide (Sigma Cat#F4799) diluted to a final concentration of 150 mg/mL in 750 mL TBS Buffer (50 mM Tris-HCl, pH 7.4, with 150 mM NaCl) for 1 h at 4°C on a roller. The supernatants were removed and the eluates were concentrated in Amicon Ultra-0.5 mL 3K MWCO filters (Sigma Cat#UFC5003) according to the manufacturer's recommendations. Samples were loaded and migrated on Novex 16% Tris Glycine Precast Gels (Invitrogen Cat#XP00162BOX). Silver stains were performed on the gels using the Pierce Silver Stain Kit (Thermo Fisher Scientific Cat#24612) according to the manufacturer's instructions. Several bands were excised for mass spectrometry.

Proteomics and Mass Spectrometry Analysis

IP enriched proteins of full-length kinetochore protein IPs and control samples were separated on 10% NuPAGE 10% Bis-Tris protein gel (Invitrogen Cat#NP0301BOX) and stained with colloidal blue (LabSafe GEL Blue GBiosciences Cat#786-35). SDS-PAGE was used with short separation as a clean-up step, and 4 gel slices were excised. Gel slices were washed and proteins reduced with 10 mM DTT (Euromedex, Cat#EU0006-B) prior to alkylation with 55 mM iodoacetamide (Sigma Cat#I6125). After washing and shrinking the gel pieces with 100% MeCN (Merck Cat#1.00099), in-gel digestion was performed using trypsin/Lys-C (Promega Cat#V5071) overnight in 25 mM NH_4HCO_3 (Fluka, Cat#09830) at 30°C. Peptides were then extracted using 60/35/5 MeCN/H_2O/HCOOH (Fluka Cat#94318) and vacuum concentrated to dryness. Protein on beads samples (CENP-T-HFDextension IP and CENP-T and Dsn1 antibody validations) were washed twice with 100 mL of 25 mM NH_4HCO_3 and submitted to on-beads digestion with 0.2 mg of trypsin/Lyc-C for 1h. Digested sample were then loaded onto homemade C18 StageTips for desalting and peptides were eluted using 40/60 MeCN/H_2O + 0.1% formic acid and vacuum concentrated to dryness. Gel samples were chromatographically separated using an RSLCnano system (UltiMate 3000 RSLCnano, Thermo Fisher Scientific) coupled to an Orbitrap Fusion mass spectrometer (Q-OT-qIT, Thermo Fisher Scientific with a Nanospay Flex ion source (Thermo Fisher Scientific) and bead samples were also analyzed with a Q Exactive HF-X mass spectrometer. Peptides were first trapped on a C18 precolumn (300 mm inner diameter x 5 mm; Invitrogen Cat#160454) at 20 ml/min or 2.5 mL/min with buffer A (2/98 MeCN/H_2O in 0.1% formic acid). After 3 min or 4 min of desalting, the precolumn was switched on line with the analytical C18 column (75 mm inner diameter x 50 cm; nanoViper Acclaim PepMapTM RSLC, 2 mm, 100Å, Thermo Fisher Scientific Cat#164535) equilibrated in buffer A. Separation was then performed with a linear gradient of 5% to 25% or 30% buffer B (100% MeCN in 0.1% formic acid) at a flow rate of 300 nL/min over 100 min or 91 min.

MS full scans were performed in the ultrahigh-field Orbitrap mass analyzer in ranges m/z 400–1500 or m/z 375-1500 with a resolution of 120 000 at m/z 200, ions from each full scan were HCD fragmented and analyzed in the linear ion trap or orbitrap.

For identification, the data were merged and searched against the *S. frugiperda* corn strain proteome [59] using Sequest^{HF} through Proteome Discoverer (version 2.2, Thermo Fisher Scientific) with the *S. frugiperda* CENP-T, CENP-I, CENP-N, Nsl1 candidate and Spc25 (which were all not correctly annotated in the *S. frugiperda* corn strain assembly) manually added to the proteome database. For identification of proteins in the *B. mori* IPs, the data were searched against the *B. mori* proteome. Enzyme specificity was set to trypsin and a maximum of two-missed cleavage sites were allowed. Oxidized methionine, Carbamidomethyl cysteines and N-terminal acetylation were set as variable modifications. Maximum allowed mass deviation was set to 10 ppm for monoisotopic precursor ions and 0.6 Da for MS/MS peaks. The resulting files were further processed using myProMS [56] v3.6. FDR calculation used Percolator and was set to 1% at the peptide level for the whole study.

For the kinetochore IPs on full-length lepidopteran proteins identified proteins that were at least four-fold enriched over the control (the two controls were combined) with a minimum of seven derived peptides were analyzed further (Data S1). For the *S. frugiperda* CENP-T-HFD-FLAG IP (Figure S1B) proteins that were at least four-fold enriched over the control with at least 5 derived peptides were selected for further analyses (see above). For Figure 1, known kinetochore homologs or proteins with at least seven derived peptides and that were enriched at least four-fold in three kinetochore immunoprecipitates are listed.

Immunofluorescence

Cells were grown on glass coverslips and fixed with ice cold MeOH (anti-CENP-T and anti-Spc24/25), ice cold acetone (anti-Dsn1) and 4% PFA (anti-tubulin), followed by permeabilization using 0.3% Triton X-100 in PBS and blocked in 3% BSA-PBS. The following antibodies were used: rabbit polyclonal anti-CENP-T (this paper, rabbit 045), rabbit polyclonal anti-Spc24/25 (this paper, rabbit 1621016) and polyclonal rabbit anti-Dsn1 (this paper, rabbit 1615031) generated by Covalab (Villeurbanne, FR) at the dilution 1:1000, anti-a-tubulin monoclonal Alexa Fluor 488 (Thermo Fisher Scientific Cat#53-4502-80; RRID:AB_1210526) at 1:1000, anti-FLAG M2 mouse monoclonal (Sigma Cat#F1804; RRID:AB_262044) at 1:1000, anti-phospho Histone H3-Ser10 rat monoclonal (Sigma Cat#MABE939) at 1:1000. For fluorescent conjugated secondary antibodies, we used goat anti-rabbit IgG Alexa Fluor 568 (Thermo Fisher Scientific Cat#A-11011; RRID:AB_143157) at 1:1000, goat anti-rat IgG Alexa Fluor 568 (Thermo Fisher Scientific Cat#A-11077; RRID:AB_2534121) at 1:1000, goat anti-rat IgG Alexa Fluor 488 (Thermo Fisher Scientific Cat#A-11006; RRID:AB_2534074) at 1:1000, goat anti-mouse IgG Alexa Fluor 488 (Thermo Fisher Scientific Cat#A-11029; RRID:AB_2534088) at 1:1000, goat anti-mouse IgG Alexa Fluor 568 (Thermo Fisher Scientific Cat#A-11004; RRID:AB_2534072) at 1:1000 and goat anti-rat IgG Alexa Fluor 633 (Thermo Fisher Scientific Cat#A-21094; RRID:AB_2535749) at 1:1000. DNA was stained with DAPI (Sigma Cat#D9542) and samples were mounted in Vectashield Antifade Mounting Medium (Vector Laboratories Cat# H-1000; RRID:AB_2336789).

For anti-tubulin staining cells were fixed three and five days after RNAi-mediated depletion using a protocol for the preservation of the whole cytoskelon [77]. Cells were washed with PBS for 5 minutes, then incubated for 10 min at room temperature in 1 mM dithiobis(succinimidyl propionate, DSP) (Thermo Fisher Scientific Cat#22585) in Hank's balanced salt solution (HBSS) (GIBCO Cat#14025050), followed by an incubation for 10 min at room temperature in 1 mM DSP in microtubule-stabilizing buffer (MTSB). Cells were next washed for 5 min in 0.5% Triton X-100 in MTSB and then fixed in 4% PFA in MTSB for 15 min at room temperature. After a 5 min wash in PBS, cells were incubated for 5 min in 100 mM glycine in PBS, then washed again in PBS for 5 minutes and finally nuclei were stained with DAPI (Sigma Cat#D9542) and samples were mounted in Vectashield Antifade Mounting Medium (Vector Laboratories Cat# H-1000; RRID:AB_2336789).

Microscopy

Images were acquired on Zeiss Axiovert Z1 light microscope. Z sections were acquired at 0.2 mm steps using 100X 1.4 NA oil objective.

Quantification of fluorescence intensity was performed using the Fiji software [57] on unprocessed TIFF images. Mitotic cells (H3S10ph positive) were quantified. For RNAi depleted cells, we first annotated the cells using an automated system (kind gift from Solène Hervé, Fachinetti lab, UMR144, Institut Curie, Paris, France). H3S10ph signals were then used as markers to manually select, using the freehand selections tool, the nuclear area. The mean fluorescence intensity of each nucleus was measured and corrected for background. For background correction, the average of mean intensities of three random circular regions of fixed size (30x30 pixels) placed outside nuclear areas was determined.

To quantify the fluorescent signal intensities for LacO/LacI tethering assays, the mean fluorescence intensities of CENP-T, Dsn1 and Spc24/25 signals were first measured in circular regions of fixed size (10x10 pixels) overlapping GFP-LacI fusion protein foci (visualized by the GFP signals). Then, the mean fluorescence intensity of CENP-T, Dsn1 and Spc24/25 at endogenous loci was determined as the average in three random circular regions of fixed size (10x10 pixels) placed over the mitotic chromosome. As before, the background intensity was also measured as the average of mean fluorescence intensities of three random circular regions of fixed size (10x10 pixels). Both the mean fluorescence intensities overlapping the GFP foci or the endogenous loci were corrected with this background value. For the quantifications in Figure 4, the ratio between the mean fluorescence intensity over the GFP foci and over endogenous loci was calculated and plotted. A ratio above 1 means that the respective kinetochore components are enriched over GFP fusion protein foci and therefore indicates recruitment by the tethered protein. In contrast, a ratio around 1 or below indicate that kinetochore components are not preferentially enriched or are even depleted over the GFP fusion protein foci compared to

endogenous loci. While the corrected values of the fluorescence intensities at the endogenous loci were always positive, the corrected fluorescence intensities overlapping the GFP foci can be negative in cases where the immunosignal was low and even below the average background intensity. Therefore, the ratio of (corrected immunosignal overlapping the GFP foci/ corrected intensities at the endogenous loci) can be negative.

For statistical analysis the Mann-Whitney test (unpaired, non-parametric test) was used to compare two ranks, using GraphPad Prism version 8.12 for Mac (GraphPad Software, https://www.graphpad.com/scientific-software/prism/). Differences were considered statistically significant at values of P values **%** 0.05.

RNAi-mediated knock-down

BmN4-SID1 cells were grown on coverslips and incubated with 400pg/ml dsRNA for three days. After three days, the medium was change to add another 400pg/ml dsRNA. After three or five days, cells were fixed and processed for IF as described. Primers used to generate the DNA templates fused to T7 promoter for dsRNA generation are listed in Table S5.

RNA blot analyses

Total RNA was isolated using TRIzol (Invitrogen Cat#15596018) following the manufactor's instruction. RNA blots were performed using around 10 mg total RNA (CENP-T, CENP-I, CENP-N, Nsl1, Mis12, Spc25) or polyA-selected mRNAs from 20 mg total RNA (CENP-M, Spc24) per lane. RNA samples from cells incubated for five days with respective dsRNAs were treated with glyoxal using NorthernMax-Gly Sample Loading Dye (Thermo Fisher Scientific Cat#AM8551). The samples were loaded on a 1% agarose gel prepared using NorthernMax-Gly Gel Running Buffer (Thermo Fisher Scientific Cat#AM8678) according to the manufacturer's instructions. The RNA was blotted onto a Nytran membrane in 20X SSC (175.3 g NaCl, 88.2 g sodium citrate in 1.0 l water adjusted to pH 7) using the TurboBlotter System (Bio-Rad Cat#1704155). After UV crosslinking RNA to the membrane, glyoxal treatment was reversed by incubating the membrane in 10 mM Tris-HCl pH 8 for 20 minutes at room temperature. The membrane was incubated in 12 mL QuickHyb solution (Agilent Cat#201220) with 1.0 mg salmon-sperm ssDNA (Sigma Cat#31149) for 1 hour at 65°C. Body-labeled antisense riboprobes against kinetochore mRNAs and the loading control were prepared by using PCR products as templates for *in vitro* transcription (MAXIscript T7 Transcription kit, Thermo Fisher Scientific Cat#AM1312). A radiolabeled probe against *B. mori* Rpl32 mRNA served as loading control. After an overnight hybridization at 65°C with radio-labeled probes, the membrane was washed twice in 2X SSC, 0.1% SDS for 5 minutes and once in 0.2X SSC, 0.1% SDS for 30 minutes. The membranes were exposed to phosphoimaging plates and analyzed using a Typhoon TRIO Imager.

CRISPR-mediated genome editing in B. mori

The non-diapause strain N4 maintained at the University of Tokyo was used. All larvae were fed with fresh mulberry leaves or artificial diet SilkMate (NOSAN SilkMate PS) under a continuous cycle of 12-h light and 12-h darkness at 25°C. Unique single-guide RNA (sgRNA) target sequences in the silkworm genome were selected using CRISPRdirect (https://crispr.dbcls.jp/) [58]. The sequence specificity in N4 strain was also checked by SilkBase (http://silkbase.ab.a.u-tokyo.ac.jp) [61]. Primers used for sgRNA transcription *in vitro* are listed in Table S5. The sgRNA was transcribed *in vitro* according to a method reported previously [78]. A mixture of sgRNA (400 ng/mL) and Cas9 Nuclease protein NLS (120 ng/mL; NIPPON GENE Cat#319-08641) in injection buffer (100 mM KOAc, 2 mM $Mg(OAc)5_2$, 30 mM HEPES-KOH; pH 7.4) was injected into each egg within 3 h after oviposition [79]. The injected embryos were incubated at 25°C in a humidified Petri dish until hatching. Injected individuals were crossed with non-injected individuals to obtain G_1 broods. To identify G_1 moths in which mutant alleles were transmitted from G_0, genomic DNA was extracted from a G_1 adult leg using the hot sodium hydroxide and Tris (HotSHOT) method [44]. Genomic PCR was performed using KOD One™ (TOYOBO Cat# KMM-101) under the following conditions: 35 cycles of denaturation at 98°C for 10 s, annealing at 60°C for 5 s, extension at 68°C for 5 s. Primers used for mutation screening are listed in Table S5. The PCR products were denatured and reannealed at 95°C for 10 min, followed by gradual cooling to 25°C. Mutations at the target site were detected by heteroduplex mobility assay using the MultiNA microchip electrophoresis system (SHIMADZU) with the DNA-500 reagent kit (SHIMADZU Cat#292-27910-91) [80, 81]. A mutation at the target site was sequenced using BigDye® Terminator v3.1 Cycle Sequencing Kit (Applied Biosystems Cat#4337454) and ABI PRISM® 3130xl Genetic Analyzer (Applied Biosystems). We maintained the mutant line and obtained eggs carrying the homozygous mutation by crossing between two heterozygous mutants.

QUANTIFICATION AND STATISTICAL ANALYSIS

Statistical details of experiments are detailed in the Figure legends, including the number of biological replicates (n = number of cells), the definition of center, dispersion and precision measures (mean, SEM and SD). Statistical analyses were performed with GraphPad Prism 8.12 for Mac.

DATA AND CODE AVAILABILITY

The mass spectrometry proteomic datasets generated during this study are available at the ProteomeXchange Consortium via the PRIDE [82] partner repository with the dataset identifier PRIDE: PXD016092 (username: reviewer44001@ebi.ac.uk, password: on7Kq9rP).